UNIVERSITY OF KWAZULU-NATAL

FACULTY OF SCIENCE & AGRICULTURE

School of Physics

AN INVESTIGATION OF HIGH VELOCITY FLOWS IN HF RADAR DATA DURING NORTHWARD INTERPLANETARY MAGNETIC FIELD, NON-SUBSTORM INTERVALS

BY

ZOLILE MTUMELA

A thesis submitted as the dissertation component in partial fulfillment of the academic requirements for the degree of Master of Science in the school of physics, University of KwaZulu-Natal, Durban

JULY 2010

An investigation of high velocity flows in HF radar data during northward interplanetary magnetic field, non-substorm intervals

by

Zolile Mtumela

A thesis submitted as the dissertation component
in partial fulfillment of the academic
requirements for the degree of
Master of Science in the
School of Physics,
University of KwaZulu-Natal
Durban

July 2010

As the candidate's Supervisor I have/have not approved this thesis for submission.

Signed: …….. Name …….. Date ……..

As the candidate's Co-supervisor I have/have not approved this thesis for submission.

Signed: …….. Name …….. Date ……..

ABSTRACT

Several previous studies, including one using early Sanae radar data, have found examples of high speed ionospheric plasma flows on the nightside, mapping to the magnetospheric tail, during periods which were magnetically quiet. These high speed flows were interpreted to be associated with the release of energy from a rapid reconfiguration of tail magnetic field lines due to reconnection. Such events are now known as 'TRINNIs' or 'tail reconnection during IMF northward, non-substorm intervals'. The purpose of this study was to identify further TRINNI events, using SuperDARN data from both hemispheres. In situations where the *y*-component of the Interplanetary Magnetic Field dominates over the *z*-component, the directions of both the high speed flows and the underlying convection pattern depend on the direction of the *y*-component. Some examples of likely TRINNI events for cases where the *y*-component was positive and negative are presented and discussed. The assumption of a non-substorm interval is justified by magnetometer and GOES satellite data, and the observations are discussed in relation to magnetic reconnection in the magnetotail.

PREFACE

The experimental work described in this dissertation was carried out in the School of Physics, University of KwaZulu-Natal, Durban and at the Hermanus Magnetic Observatory, Hermanus, from January 2008 to December 2009, under the supervision of Professor J.P.S Rash and Dr P.R Sutcliffe.

These studies represent original work by the author and have not otherwise been submitted in any form for any degree or diploma to any tertiary institution. Where use has been made of the work of others it is duly acknowledged in the text.

DECLARATION - PLAGIARISM

I, ……., declare that

1. The research reported in this thesis, except where otherwise indicated, is my original work research.

2. This thesis has not been submitted for any degree or examination at any other university.

3. This thesis does not contain other persons' data, pictures, graphs or other information, unless specifically acknowledged as being sourced from other persons.

4. This thesis does not contain other persons' writing, unless specifically acknowledged as being sourced from the researchers. Where other written sources have been quoted, then:
   a. Their words have been re-written but the general information attributed to them has been referenced.
   b. Where their exact words have been used, then their writing has been placed in italics and inside quotation marks, and referenced.

5. This thesis does not contain text, graphics or tables copied and pasted from the Internet, unless specifically acknowledged, and the source being detailed in the thesis and in the References sections.

Signed: ……

ACKNOWLEDGEMENTS

I would like to extend my thanks to the profound undermentioned persons, each of whom has made this research work possible.

Firstly, I would like to thank my Supervisor Professor J.P.S Rash for his time, patience, expert guidance and all the necessary insight throughout the work.

Secondly, many thanks to Dr P.R Sutcliffe for his role in his capacity of being a Co-supervisor, giving guidance, suggestions throughout the work.

My great thanks to the space physics group (SHARE group), particularly Dr E. Mravlag for his tireless assistance on the HF Radar processing computers, providing data for me, and Dr J.A.E. Stephenson for her assistance during the course of this work.

My sincere thanks to my family for giving me an opportunity to proceed with my studies and their unfailing support and to my friends and colleagues for their encouragement, motivation and assistance.

My great thanks to the HMO as a facility of the NRF for financial support.

CONTENTS

LIST OF FIGURES

LIST OF TABLES

CHAPTER 1

INTRODUCTION

1.1 The Earth's magnetosphere

A planet's magnetosphere is defined as the region of space around the planet where the planet's magnetic field dominates over interplanetary effects. A simple sketch of the Earth's magnetosphere is shown in Fig. 1.1, which represents a noon-midnight cross-section with the sun to the left of the figure. The solar wind is a continuous flow of ionized gases which blows outward from the sun typically at about 400 km/s and varies in velocity and density with the amount of surface activity on the sun. The source of the solar wind is the sun's hot corona, the sun's outer atmosphere. The magnetic field embedded in the solar wind is called the interplanetary magnetic field (IMF), which consists of 'open' field lines originating in the sun. Because of the supersonic speed of the solar wind and the 'shield' provided by the Earth's magnetic field, a shock wave called the bow shock is generated which deflects the oncoming solar wind and prevents it from reaching Earth's surface. The bow shock arises as the supersonic solar wind encounters the obstacle formed by the Earth's magnetic field. Inside the bow shock is a region, called the magnetosheath, where the solar wind flows at subsonic speed around the magnetosphere. Behind the bow shock, the magnetic bubble called the magnetosphere is formed. The bounding surface of the magnetosphere is called the magnetopause. The magnetopause is the boundary between the magnetosheath and magnetosphere, typically located at a distance of about 10 R_E (Earth radii) on the sunward side (Burgess, 1995).

On the nightside of the Earth, the magnetic field lines are swept back to form a tail with a length > 1000 R_E and roughly circular cross-section called the magnetotail. The equatorial region of the magnetotail contains a sheet of plasma, called the plasma sheet. The magnetotail consists of two low density regions known as the tail lobes, one in the north half of the magnetotail and the other in the south half of the magnetotail. The field in the lobes is typically B ~20 nT. The two lobes are separated

by a neutral sheet in which there is a small but finite normal magnetic field component (Hughes, 1995).

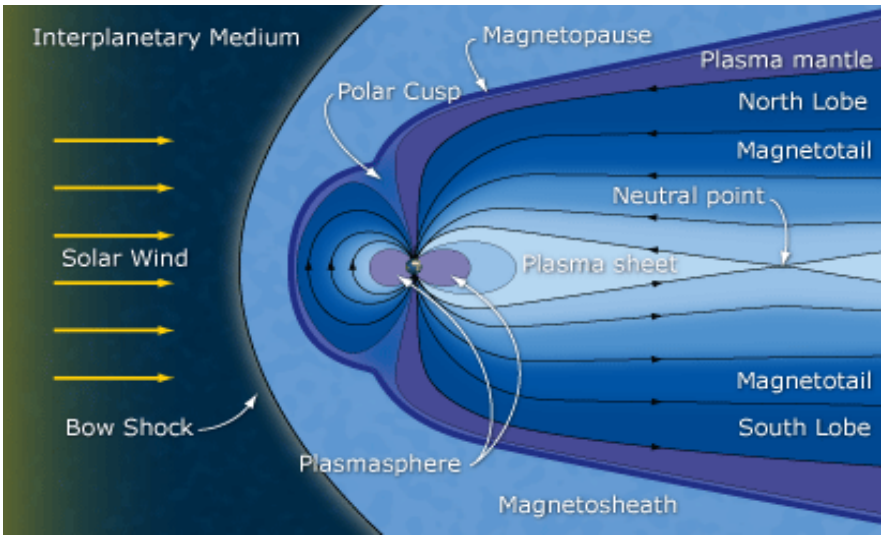

Fig. 1.1: Schematic representation of the Earth's magnetosphere (from http://clusterlaunch.esa.int/science-e/www/object/index.cfm?fobjectid=41918).

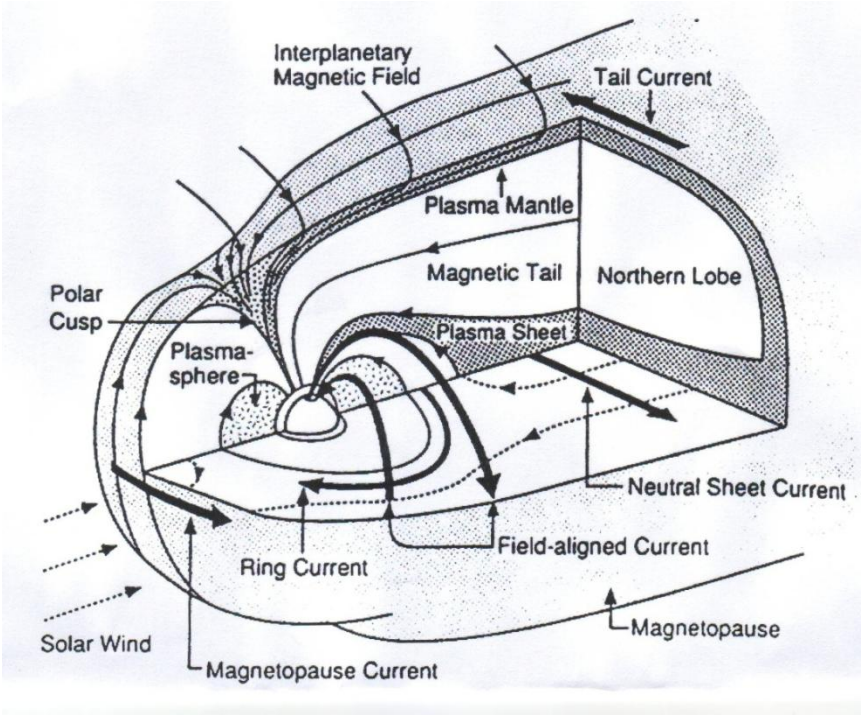

Fig. 1.2: Schematic view of the Earth's magnetosphere in 3-dimensions (from Russell et al., 1997).

A neutral sheet current flows from the dawn to dusk flanks across the neutral sheet and closes around the surface of the tail, as indicated in the three-dimensional representation of the magnetosphere shown in Fig. 1.2. Within the lobes the plasma undergoes a $\vec{E}\times\vec{B}$ drift towards the neutral sheet. The plasmasphere is a region of dense (tens of thousands of particles per cubic centimeter) and cold (~ eV) plasma that occupies roughly the same region of the inner magnetosphere as the ring current (Wolf, 1995).

Therefore, the magnetosphere of Earth is a region in space whose shape is primarily determined by the distortion of Earth's internal magnetic field by the solar wind plasma and the interplanetary magnetic field (IMF). The properties of the magnetosphere are strongly affected by variations in the solar wind and interplanetary magnetic field. The interaction between solar wind, interplanetary magnetic field and magnetosphere is of fundamental importance in space physics.

1.2 Magnetic reconnection

The primary mechanism in the transfer of energy and momentum from the solar wind to the magnetosphere and the ionosphere is magnetic reconnection. Magnetic reconnection is the process whereby magnetic field lines from different magnetic domains are spliced to one another, changing their patterns of connectivity with respect to the sources as shown in Fig. 1.3. Domains in magnetic plasma are separated by separatrix surfaces: curved surfaces in space that divide bundles of flux. Hence each field line generally starts at a north magnetic pole and ends at a south pole, the most general way of dividing simple flux systems involves four domains separated by two separatrices: One separatrix surface divides the flux into two bundles, each of which shares a south pole, and the other separatrix surface divides the flux into two bundles, each of which shares a north pole. The intersection of the separatrices forms a separator. This type of magnetic reconnection is called the separator reconnection, in which four magnetic domains exchange magnetic field lines.

In the 2 dimensional case with non-zero northward magnetic field B_z, the relevant magnetic field lines have a X-line nature. In an ideal magnetohydrodynamics (MHD) picture, field lines and associated

plasma flow inward from above and below the separator, reconnect, and spring outward horizontally (http://en.wikipedia.org/wiki/Magnetic_reconnection).

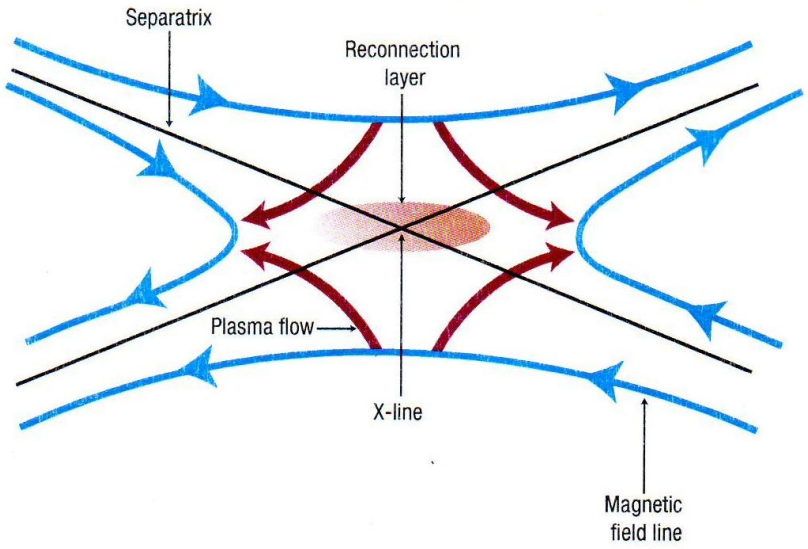

Fig. 1.3: Magnetic reconnection: This view is a cross-section through four magnetic domains undergoing separator reconnection (from Finn et al., 2006).

The solar wind interaction with the Earth's magnetic field is relatively well understood in two-dimensions, but only partially understood in three-dimensions.

1.3 Magnetospheric convection

The plasma flows seen in the polar and auroral ionospheres map out to and are driven by magnetospheric flows. The flow pattern is roughly stationary in a sun-fixed coordinate system, so that any observatory will detect variation as it rotates under the plasma flow. This double-vortex flow looks similar to thermal driven flow cells, and so the term "convection" became attached to it. One can map this flow along flux tubes using the frozen-in-flux concept and consider the corresponding magnetospheric flow.

For “frozen-in-flux”, if the conductivity of plasma is sufficient high then the motion of the plasma and the magnetic field are effectively “frozen” together. Movement of the plasma relative to the magnetic field induces a current which, from Lenz’s law, results in a $\vec{j} \times \vec{B}$ force opposing the motion. In the limit of $\sigma = \infty$ the restoring force is infinite and the motion is arrested. The plasma and magnetic field are coupled in such a way that if two elements of the plasma lie on a given field line at some instant, then they remain on the same field line at all other times irrespective of deformation in the plasma or field.

The “frozen in field” concept can be derived from Maxwell’s equations as follows. At low frequencies the displacement current is neglected in Ampere’s law:

$$\nabla \times \vec{B} = \mu_0 \vec{j} + \mu_0 \varepsilon_0 \frac{\partial \vec{E}}{\partial t} \rightarrow \mu_0 \vec{j} \qquad (1)$$

In the rest frame of the plasma ($\vec{v} = 0$), Ohm’s law is

$$\vec{j} = \sigma(\vec{E} + \vec{v} \times \vec{B}) = \sigma \vec{E} \qquad (2)$$

Substituting (2) into Faraday’s law,

$$\frac{\partial \vec{B}}{\partial t} = -\nabla \times \vec{E} = -\nabla \times \frac{\vec{j}}{\sigma}$$

and using Ampere’s law (1)

$$\frac{\partial \vec{B}}{\partial t} = -\frac{\nabla \times \nabla \times \vec{B}}{\mu_0 \sigma} = \frac{1}{\mu_0 \sigma}[\nabla(\nabla \bullet \vec{B}) - \nabla^2 \vec{B}]$$

So that $\frac{\partial \vec{B}}{\partial t} = \frac{\nabla^2 \vec{B}}{\mu_0 \sigma}$, since $\nabla \bullet \vec{B} = 0$

which describes the diffusion of the magnetic field out of the plasma.

When $\sigma = \infty$, $\partial \vec{B} / \partial t \rightarrow 0$ and the field is frozen into plasma, which is the situation in the solar wind and Earth’s magnetosphere, where σ is very large.

For simplicity, assume that the interplanetary field is directed predominantly southward, as is illustrated in Fig. 1.4. The magnetic field driven by the solar wind flow against the sunward side of the magnetosphere will be antiparallel to the geomagnetic field on the other side of the magnetopause. Suppose that a magnetic X-line forms there and that reconnection occurs between the field lines labeled 1 and 1'. The resulting field lines, while remaining attached to the ionosphere, are dragged along with the magnetosheath flow to the nightside magnetosphere where, in the tail, the magnetic configuration invites formation of a second X-line. The configuration of magnetic field lines in the Earth's magnetosphere is determined by magnetic reconnection between the interplanetary magnetic field and the geomagnetic field. This gives a clear indication that magnetospheric convection is driven primarily by magnetic reconnection (Hughes, 1995).

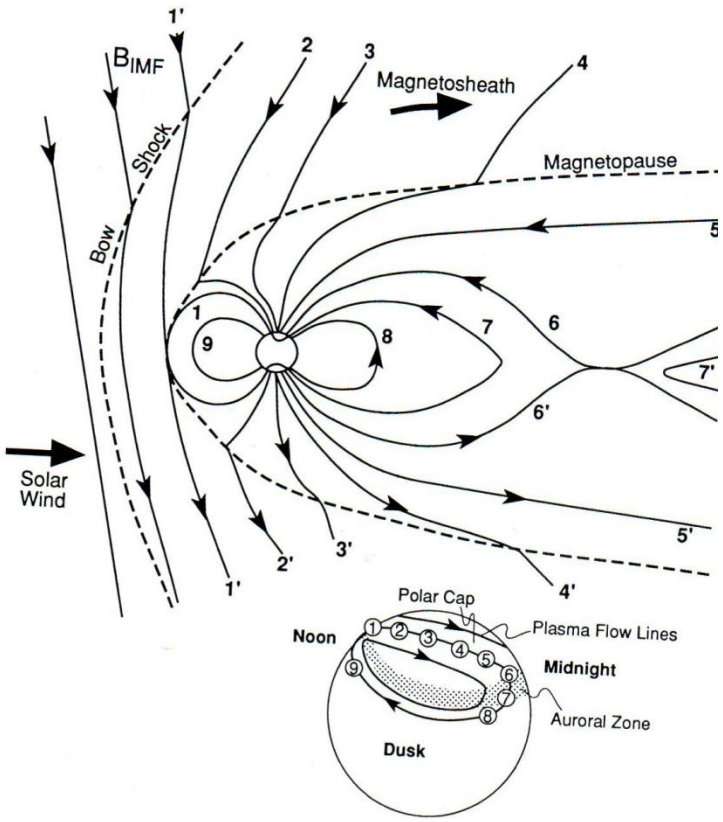

Fig. 1.4: Shows the flow of plasma within the magnetosphere (convection) driven by magnetic reconnection. The numbered field lines show a succession of configurations of a geomagnetic field line (from Hughes, 1995). The inset shows the resulting plasma flow in the polar ionosphere.

Because of the different magnitudes of the gyrofrequencies of electrons and ions in the ionosphere, due to their difference in mass, the electrons move with the field lines while the ions do not. Thus the circulating currents known as 'ionospheric convection' are set up as shown in Fig. 1.5. The direction of circulation is shown in the bottom 'inset' in Fig. 1.4. Associated with this circulation is an electric field, with the convection flow along equipotentials. Because the currents are due to motion of the electrons, the direction of convectional current flow, shown in Fig. 1.5, is in the opposite direction.

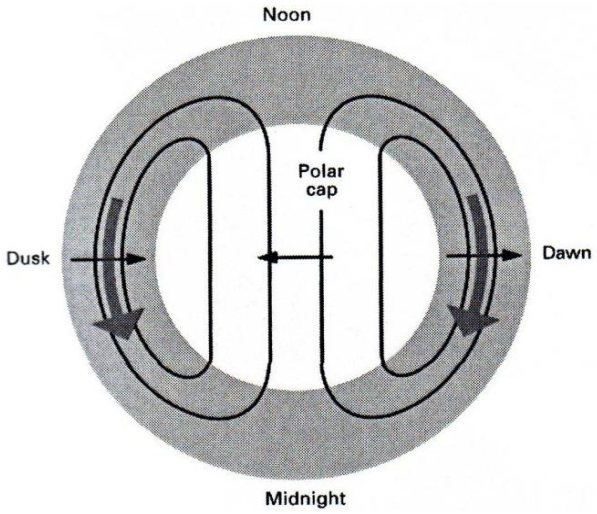

Fig. 1.5: Schematic diagram of the equipotentials of the ionospheric electric field in the northern hemisphere auroral oval, the shaded area (from Biskamp, 2000).The light arrows indicate the electric field direction and heavy arrows the ionospheric convection current.

These convection patterns were first derived from magnetometer measurements, but are now observed in real time with the SuperDARN radars described in section 1.5. The "two cell" pattern shown in Fig. 1.5 is observed during southward IMF, when reconnection occurs at the upstream side of the magnetosphere. For northward IMF the pattern is less structured, and reconnection may take place in the lobes. Also, when the y component of the IMF dominates over the z component, the cell pattern is distorted, with the noon separator between the cells moving towards dawn or dusk, and opposite effects in the northern and southern hemispheres.

Thus, if B_y is positive (negative) the noon separator moves towards dawn (dusk) in the northern hemisphere and dusk (dawn) in the southern hemisphere (Grocott et al., 2004).

1.4 Substorms

Substorms are magnetospheric disturbances that occur when the interplanetary magnetic field turns southward, allowing interplanetary and terrestrial magnetic field lines to merge at the dayside magnetopause. Substorms have been divided into three phases: growth phase, expansion phase and recovery phase. During the growth phase energy is transferred from the solar wind to the magnetosphere, the tail lobe field increases and the near earth plasma sheet is compressed.

The Near-Earth Neutral Line model assumes that at substorm onset (the start of the expansion phase) reconnection takes place between the oppositely directed field lines above and below the current sheet at a distance of about 20-30 R_E down the magnetotail. When reconnection starts, it may take a while before it reaches the open field lines of the lobe. The closed field line reconnection may provide many substorm-like signatures before the main substorm onset. The observed high speed flows are naturally explained by this model. The injection of high energy particles into the ring current due to magnetic field reconfiguration are considered to be one of the most common and reliable indicators of substorm onset. The cross-tail current disruption and the formation of the Substorm Current Wedge are considered to be secondary effects. Substorm Current Wedge is a current diverted through a circuit consisting of earthward field-aligned currents on the eastern side of the wedge, a westward auroral electroject in the ionosphere, and tailward field-aligned currents on the western side of the wedge. The current disruption leading to the Substorm Current Wedge formation is acting on a current sheet that has been enhanced and propagated closer to Earth during the substorm growth phase. The Substorm Current Wedge leads to the association of Pi2 pulsations at higher latitude, and this has been used as a substorm indicator. However this is not as reliable as the other indicators, namely particle injection and evidence of the westward auroral electroject seen in ground magnetometer measurements as a large decrease in the northward (X) component of the field. (Rostoker et al, 1980 & http://www.oulu.fi/~spaceweb/~spaceweb /textbook/substorms/).

1.5 The SuperDARN radars

The SuperDARN (Dual Auroral Radar Network) is an international array of HF (8 – 20 MHz) coherent radars spanning the auroral regions of both the northern and the southern hemisphere (Greenwald et al., 1995). At the present, the northern hemisphere network consists of eleven radars and the southern hemisphere network consists of seven radars. Further details of the radars will be given in the next chapter.

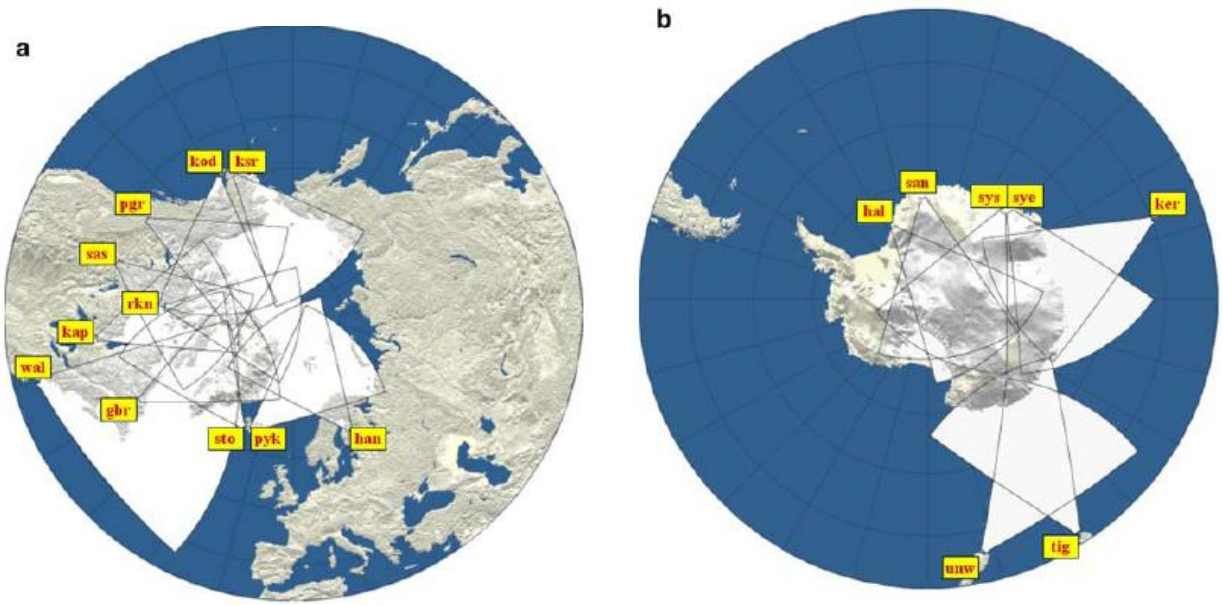

(a) Northern hemisphere (b) Southern hemisphere

Fig. 1.6 : SuperDARN Radars with their respective fields of view, (a) northern hemisphere radars based in the Arctic region of the Earth and (b) southern hemisphere radars located in the Antarctic region and its nearby islands (from Chisham et al., 2007). The code name of each radar is highlighted in red close to the radar location. Full details of the radars are provided in Table 1.1.

The transmitted high frequency (HF) radar waves are refracted in the ionosphere and can therefore achieve perpendicularity to the Earth's magnetic field over large areas in polar latitudes. This enables SuperDARN to obtain global convection maps of the ionospheric plasma motions driven by magnetospheric processes.

The use of HF frequencies means that the SuperDARN radars measure the Doppler velocity of metre-scale F-region irregularity backscatter targets (Walker et al., 1987) moving with the ambient plasma at the $\vec{E}\times\vec{B}$ convection velocity. The convection velocity $\vec{v}$ is related to potential Φ through the relationships

$$\vec{E} = -\Delta\Phi \tag{3}$$

and

$$\vec{v} = \frac{\vec{E}\times\vec{B}}{B^2} \tag{4}$$

This was the approach used by Ruohoniemi and Baker (1998) in developing the 'Map Potential' technique to find a functional form for the distribution of electrostatic potential in the ionosphere, Φ, that 'best fit' all the line-of-sight velocity measurements at the time of interest. The global convection maps are generated at the 2 minute time resolution of the radar scans (more recently the standard scan time has been reduced to 1 minute), which is suitable for observing the response of ionospheric convection to changes in the solar wind and the interplanetary magnetic field (IMF).

Table 1.1: Details of the SuperDARN radars

Radar Name	Code	Geographic Latitude	Geographic Longitude
Northern Hemisphere			
Goose Bay	Gbr	53.32° N	60.46° W
Kapuskasing	Kap	49.39° N	82.32° W
Saskatoon	Sas	52.16° N	106.53° W
Stokkseyri	Sto	63.86° N	22.02° W
Hankasalmi	Han	62.32° N	26.61° E
Pykkvibaer	Pyk	63.86° N	19.20° W
Kodiak	Kod	57.60° N	152.20° W
Prince George	Pgr	53.98° N	122.59° W
Kind Salmon	Ksr	58.68° N	156.65° W
Wallops Island	Wal	37.93° N	75.47° W
Rankin Inlet	Rkn	62.82° N	93.11° W
Southern Hemisphere			
Halley (SHARE)	Hal	72.52° S	26.63° W
Sanae (SHARE)	San	71.68° S	2.85° W
Syowa South	Sys	69.00° S	39.58° E
Syowa East	Sye	69.01° S	39.61° E
Kerguelen	Ker	49.35° S	70.26° E
TIGER Tasmania	Tig	43.38° S	147.23° E
TIGER Unwin	Unw	46.51° S	168.38° E

1.6 Scientific motivation

As discussed earlier, magnetic reconnection plays a major role in the transfer of energy, momentum and plasma from the solar wind into the magnetospheric system. The global convection pattern in the ionosphere depends strongly on the orientation of the interplanetary magnetic field (IMF), which supports the idea that the major driving mechanism of ionospheric convection is merging (or reconnection) of the IMF and geomagnetic field (e.g. Watanabe et al., 2007). The B_z –component of the interplanetary magnetic field is a key parameter which determines whether the magnetosphere is 'open' or 'closed', and where reconnection is likely to occur.

When the interplanetary magnetic field points south, i.e. the GSM z component is negative ($B_z < 0$), reconnection occurs predominantly on low-latitude regions of the magnetopause between the northern and southern hemisphere cusps regions. The interplanetary magnetic field lines in the magnetosheath reconnect with closed magnetospheric magnetic field lines to generate new open geomagnetic flux. When the interplanetary magnetic field points north, i.e. the GSM z component is positive ($B_z > 0$), reconnection takes place between the interplanetary magnetic field (IMF) in the magnetosheath and open tail lobe geomagnetic field lines on the high-latitude magnetopause tailward of the cusps (Dungey, 1963). For northward IMF conditions substorm activity is believed to be reduced, which allows lobe reconnection or high-latitude reconnection to take place between lobe field lines and IMF.

Observations in the dayside ionosphere suggest that open flux tube production does not switch off entirely until the clock angle (the direction of the IMF in the y-z plane, with 0 corresponding to purely northward) falls below ~30°-40° (e.g. Sandholt et al., 1998) such that during intervals of northward, but B_Y dominated IMF, both open field line (lobe) and closed field line reconnection may be taking place (Nishida et al., 1998). On the nightside, the response to a steady dayside driving under these conditions has been observed. Senior et al. (2002) and Grocott et al. (2003, 2004) have reported SuperDARN observations of large-scale bursty flows in the nightside ionosphere during extended intervals of 45° < IMF clock angle < 90°. These flows have a recurrence time of ~1h, with substructure on tens of minutes time scales. In the dawn and dusk convection cells they take the form of surges of azimuthal flow of the order of one degree wide in latitude. No evidence of

substorm signatures was found in the tail magnetic field during these events. These types of flow bursts are now known as 'tail reconnection during IMF northward non-substorm intervals' ('TRINNIs'). Grocott et al., (2004) suggested that the ionospheric signature of a TRINNI was caused by reconfiguration of an asymmetric tail resulting from prolonged dayside reconnection between terrestrial field lines and B_y -dominated interplanetary magnetic field (IMF). However, this may not explain the observation of similar events at very small clock angles (e.g. Walker et al., 1998, 2002).

1.7 Goals of this thesis

The main goal of this study is to identify further examples of tail reconnection during IMF northward non-substorm interval events using SuperDARN HF radar data in the northern and southern hemispheres. During northward interplanetary magnetic field (IMF) and non-substorm conditions in situations where y -component of the interplanetary magnetic field dominates over the z -component, high speed flows associated with reconnection can also be observed on the nightside mapping to the magnetospheric tail. The directions of both the high speed flows and underlying convection pattern depend on the orientation of the y -component of the interplanetary magnetic field. Some examples of likely TRINNI events for cases where the y -component was positive and negative are presented and discussed. The assumption of a non-substorm interval is justified by IMAGE magnetometer data, GOES satellite data for particles and other data, and the observations are discussed in relation to magnetic reconnection in the magnetotail.

Finally, the results for the TRINNI events will be compared to other results of TRINNIs, previously reported by other authors to check the consistency of these events.

1.8 Outline of this thesis

The introduction to the SuperDARN radars is provided in Chapter 1 along with the important concepts of this study such as ionospheric convection and several key concepts such as solar wind and interplanetary magnetic field and their interaction with the Earth's magnetosphere are explained.

Chapter 2 is one of the key chapters that provides more understanding on the instrumentation of the SuperDARN radars to produce high-latitude ionospheric convection 'maps', time series plots and radar field of view plots. It also mentions the instrumentation measuring interplanetary conditions in GSM coordinates and extends to explain the instrumentation for other data used in the study such as IMAGE magnetometer data.

The background regarding this study is presented in Chapter 3. Observations of flow bursts on the nightside during quiet periods for IMF northwards are discussed. These observations of flow bursts were made using southern and northern hemisphere radars, some during extremely quiet solar wind conditions. Also discussed are other similar flow bursts observed in the study of transpolar arcs that led to the phrase TRINNIs and there is more explanation on further observations of TRINNIs obtained by other authors.

The core of this study lies in Chapter 4, where the results regarding the new observations are presented, with details of how the results were obtained and analyzed. The results are evaluated there and extended to a discussion in chapter 5.

The overall discussion of the thesis results is provided in Chapter 5. It includes the reasoning behind the interpretation of the results and its significance. It also does some comparisons to the previous work done by other authors to check consistent features of TRINNIs.

Chapter 6 presents the conclusion regarding this work. Some possible future work is described in relation to what may be done to improve and extend this work.

CHAPTER 2

INSTRUMENTATION

This chapter provides brief details of the instrumentation used in this study, which concerns two intervals: interval 1 on 07 April 2006 (02:10 – 03:10 UT) and interval 2 on 13 April 2006 (21:00 – 22:00 UT).

2.1 SuperDARN radar data

Measurements of ionospheric convection from both intervals were provided by the Super Dual Auroral Radar Network (SuperDARN) radars (Greenwald et al., 1995; Chisham et al., 2007; http://superdarn.jhuapl.edu/). The SuperDARN radars primarily image the high-latitude ionospheric convection in the Northern Hemisphere and in the Southern Hemisphere, and have been used for a wide range of other ionospheric and magnetospheric studies over the past ten years (Chisham et al., 2007). The HF radars of the system each operate on a fixed frequency selected between 8 and 20 MHz, and a phasing matrix is used to sweep the beam through 16 successive positions with azimuthal separation of 3.24°. Each beam is gated up to 75 range cells which are 45 km long in standard operation, although there is an initial range distance of 180 km for measuring backscatter from the radar. Mathematically, the distance is given by:

Distance (km) = 180 + (range-gate x 45)

The dwell time for each beam position is about 7 s which gives a full 16-beam scan that covers 52° in azimuth every 2 minutes. (More recently the standard scan time has been reduced to 1 minute.) The radars field of view is measured over 16 beams directions covering an area of about 3 x 10^6 km^2 (Greenwald et al., 1995). The parameters such as the line-of-sight (l-o-s) Doppler velocity, spectral width and backscatter power from ionospheric irregularities are routinely measured. The examination of the time evolution of line-of sight Doppler velocity (v_{LOS}) measured by each radar as a function of magnetic local time (MLT) and magnetic latitude (MLAT) allows one to pinpoint the response of high-latitude convection to changes such as IMF rotations (e.g. Chisham et al., 2007; Ambrosino et al., 2009). In the standard mode the two line-of-sight velocities measured at the intersection of the beams from two radars can be combined to provide horizontal convection velocity

vectors. Global ionospheric convection patterns and potential maps are derived by fitting the available velocity data to an expansion of the potential in terms of spherical harmonic functions (Ruohoniemi and Baker, 1998). The equipotentials of the solution represent the plasma streamlines of the modeled convection pattern. The information from the statistical model of Ruohoniemi and Greenwald (1996), parameterized by concurrent IMF conditions, is used to stabilize the solution where no data are available. A Heppner-Maynard boundary, determined from line-of-sight velocity data, is used to constrain the convection pattern at lower latitudes (Heppner and Maynard, 1987; Shepherd and Ruohoniemi, 2000). All SuperDARN radars operate continuously using coordinated sounding modes.

SuperDARN radar data for individual radars can be displayed in other useful formats, such as field-of-view ("fan") plots and time series for a specified beam and number of range gates. Examples of these various data forms will be shown in this thesis.

2.2 Geocentric Solar Magnetospheric (GSM) System

In this study, the interplanetary magnetic field (IMF) has been measured in geocentric solar magnetospheric (GSM) coordinates in both intervals, lagged by 54 minutes for interval 1 and lagged by 30 minutes for interval 2. The geocentric solar magnetospheric coordinate system is Earth centered and has its x axis pointing from the Earth towards the sun and its z axis is the projection of the Earth's magnetic dipole axis (positive north) on to the plane perpendicular to the x axis as shown in Fig. 2.1. The y axis is tangential to the Earth's orbit around the sun, opposite to the orbit direction.

The direction of the geomagnetic field near the nose of the magnetosphere is well ordered. This system is considered as the best system to use when studying the effects of interplanetary magnetic field on magnetospheric and ionospheric phenomena. Spacecraft positions and IMF components are normally conveniently specified in these GSM coordinates.

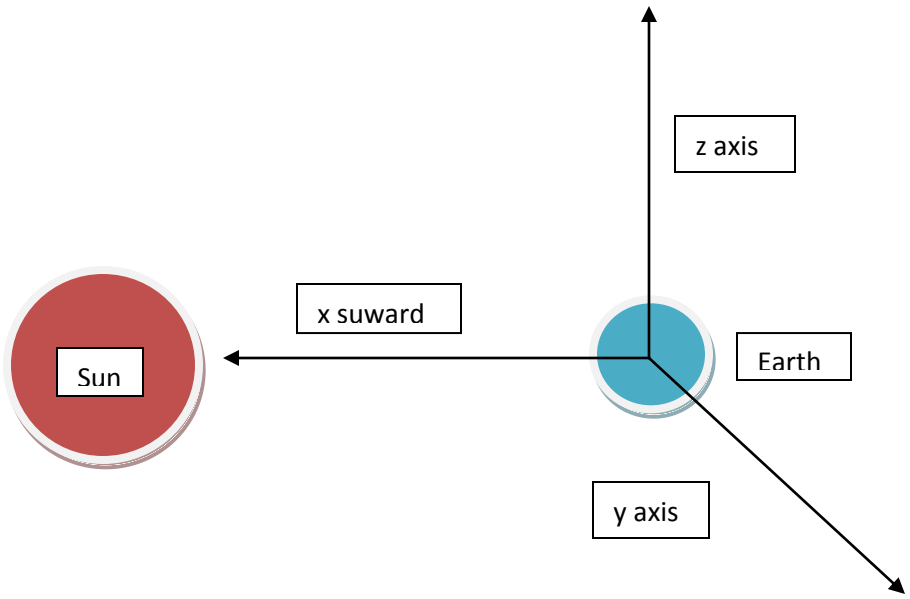

Fig. 2.1: GSM coordinates system, Earth as viewed from a point above the geographic North pole.

2.3 Interplanetary conditions

The interplanetary conditions during each interval were monitored by the ACE spacecraft (Stone et al., 1998), located at GSM coordinates (X, Y, Z) = (240, 41, -5) R_E during interval 1 on 07 April 2006 and (X, Y, Z) = (242, 35, -7) R_E during interval 2 on 13 April 2006. From the spacecraft position and the solar wind velocity the lagtime for propagation to the magnetosphere was 54 minutes for interval 1 and 30 minutes for interval 2. The IMF conditions (total B and the three GSM components) for each interval were measured by the MAG instrument (Smith et al., 1998) and solar wind conditions (velocity and density) obtained by the SWEPAM instruments (McComas et al., 1998).

The GSM coordinates for the ACE IMF data were obtained from (http://www.srl.caltech.edu/ACE/ASC/level/lvl2DATA MAG.html).

2.4 IMAGE magnetometer array

The International Monitor for Auroral Geomagnetic Effects (IMAGE) consists of 31 magnetometers maintained by 10 institutes from Finland, Norway, Poland, Russia and Sweden shown in Fig. 2.2. The stations covers geographic latitudes from 60 to 79 degrees shown in table 2.1. Table 2.1 has shown 26 stations that have been recorded during these intervals. The primary objectives of IMAGE are to study auroral electrojects and two-dimensional current systems in the northern auroral zone. About ten IMAGE stations are permanent observatories fulfilling international standards for absolute values of the field components. The other stations are considered as variometers with occasionally performed absolute measurements.

The IMAGE magnetometer data is a part of the MIRACLE ground based network which also contains 8 allsky cameras and the STARE coherent radar. MIRACLE –The Magnetometer – Ionospheric Radar – Allsky Cameras Large Experiment is a two dimensional instrument network constructed for mesoscale studies of auroral electrodynamics.

The good latitudinal coverage of the IMAGE array enables the position of the auroral electroject to be pinpointed, as well as providing indication of substorms, which is the main purpose for which it is used in this study. The position of the auroral electroject is shown by maximum disturbance of magnetic field when it is pinpointed from the MAGE array data.

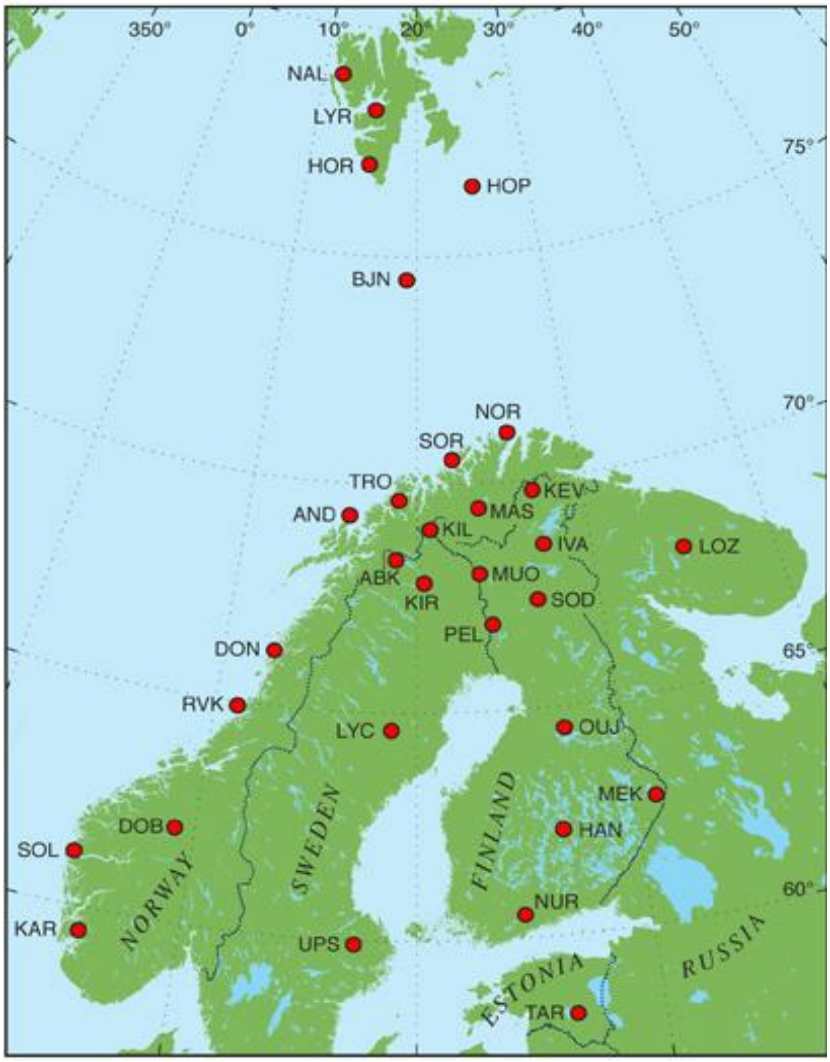

Fig. 2.2: IMAGE map for magnetometer network (from http://www.space.fmi.fi/image/stations.html)

Table 2.1: List of International Monitor for Auroral Geomagnetic Effects (IMAGE) considered in the magnetometer data in Fig. 4.10 and 4.11.

Station	Code	Geographic latitude	Geographic longitude
Ny Ålesund	NAL	78.92°	11.95°
Longyearbyen	LYR	78.20°	15.82°
Hornsund	HOR	77.00°	15.60°
Bear Island	BJN	74.50°	19.20°
Sørøya	SOR	70.54°	22.22°
Kevo	KEV	69.76°	27.01°
Tromsø	TRO	69.66°	18.94°
Masi	MAS	69.46°	23.70°
Andenes	AND	69.30°	16.03°
Kilpsjärvi	KIL	69.02°	20.79°
Ivalo	IVA	68.56°	27.29°
Abisko	ABK	68.35°	18.82°
Muonio	MUO	68.02°	23.53°
Lovozero	LOZ	67.97°	35.08°
Kiruna	KIR	67.84°	20.42°
Sodankylä	SOD	67.37°	26.63°
Pello	PEL	66.90°	24.08°
Rørvik	RVK	64.94°	10.98°
Oulujärvi	OUJ	64.52°	27.23°
Mekrijärv	MEK	62.77°	30.97°
Hankasalmi	HAN	62.30°	26.65°
Dombås	DOB	62.07°	9.11°
Nurmijärvi	NUR	60.50°	24.65°
Uppsala	UPS	59.90°	17.35°
Karmøy	KAR	59.21°	5.24°
Tartu	TAR	58.26°	26.46°

2.5 Hermanus pulsation magnetometer

The data used to check for Pi2 pulsations were obtained by measuring the voltage induced in two horizontally mounted induction sensors, one oriented approximately in the magnetic meridian (H – component) and the other perpendicular to this direction (D –component). The data are logged digitally on a personal computer with sampling at 1 s intervals and accurate timing provided by GPS receiver. The appearance of Pi2 pulsations in the data are regularly utilized by researchers world-wide to determine the occurrence and timing of substorm onsets and enhancements. However, as discussed later, Sutcliffe (1998) has shown that Pi2s can also occur when there are no substorms, so they alone cannot be relied upon as a certain indicator of substorms. Pi2 pulsations for both intervals were observed during quiet solar wind conditions where there is no evidence of substorms.

2.6 GOES satellite data

The Geostationary Operating Environment Satellites (GOES) are geostationary satellites (i.e. orbit radius 6.6 Earth radii) which carry onboard a Space Environment Monitor (SEM) system that measures x-rays, energetic particles and magnetic field at the spacecraft. The GOES system currently operates GOES-12 as the operational East Satellite located at 75° W and GOES-10 is located at 65° W. GOES-11 is designated GOES –WEST, currently located at 135° W over the Pacific Ocean. GOES satellites are able to monitor storm development and track their movements, and also provide the extremely accurate image navigation capability necessary to successfully track local areas of severe storms.

In this dissertation the GOES satellites are used to check for energetic particle injection as a more reliable indicator of substorm activity than Pi2 pulsations, as noted in the previous section. The electron (> 1 MeV) and proton (> 2 MeV and > 10 MeV) flux monitors provide the data for this check.

CHAPTER 3

BACKGROUND OF TRINNIs

3.1 Observations of flow bursts on the nightside during quiet periods for IMF northwards

Walker et al (1998, 2002) observed strong flow bursts in the southern hemisphere during extremely quiet solar wind conditions where $B < 3$ nT, $0 < B_z < 2$ nT. For the entire period the solar wind velocity was small and steady between 300 and 340 km/s. These condition exceeded the criteria defining a quiet magnetosphere developed by Kerns and Gussenhoven (1990), but met the more stringent condition of Gussenhoven (1988) of solar wind speed less than 400 km/s, $B_z < 2$ nT and $B < 5$ nT and these conditions were maintained for at least 2 to 4 hours. Flow velocities suddenly increasing to ≥ 1000 m/s for short periods characterize the flow bursts.

(a)

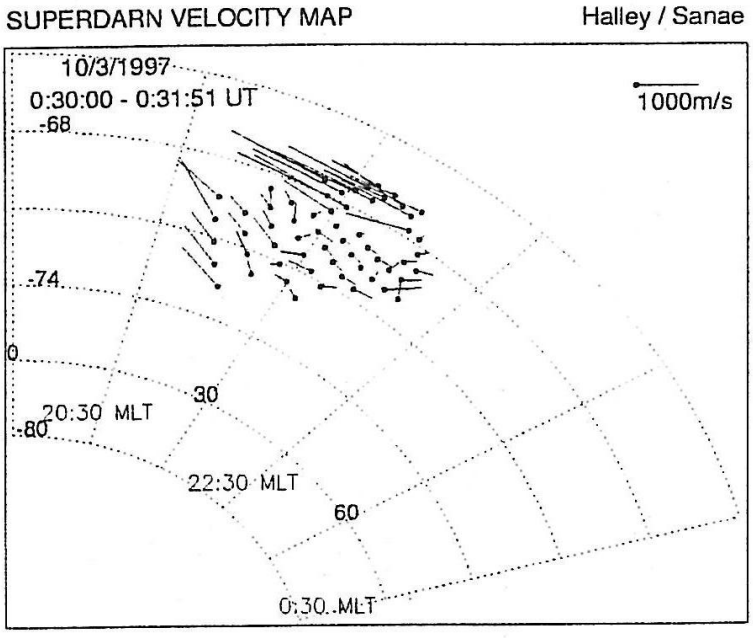

Fig. 3.1(a): Flow velocities during a flow burst (from Walker et al (1998)).

Velocities of 2000 m/s were observed for these intervals of approximately 12 minutes. Walker et al., 1998 used the HF radars at Sanae and Halley in Antarctica to show this strong activity in the nightside ionosphere.

Senior et al (2002) made similar observations in the northern hemisphere, during a period when the total magnetic field B varied between 3.0 and 4.5 nT and B_z was positive. The solar wind speed was about 350 km/s.

(b)

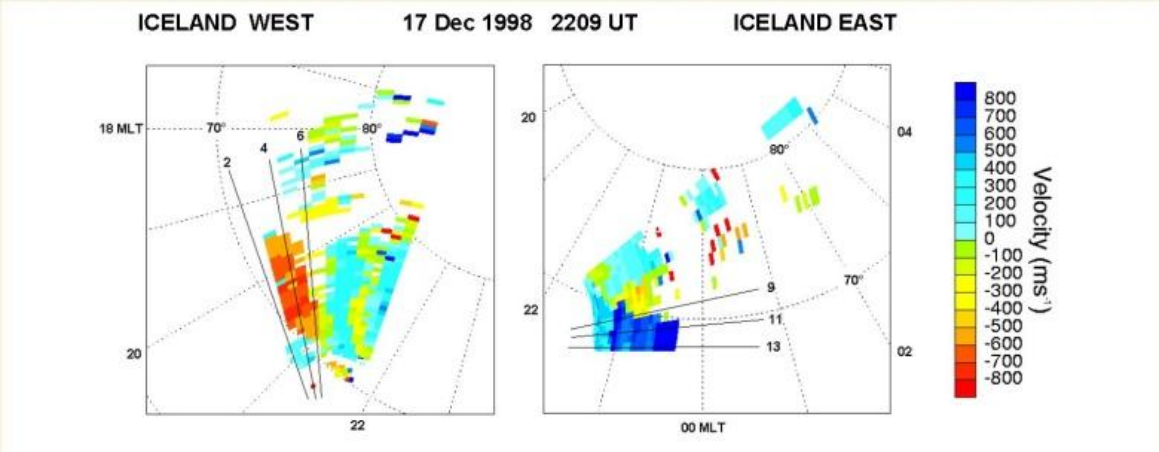

Fig. 3.1(b): Radial velocity maps from the two radar in Iceland at 22:09 UT (Iceland-west is on the left, and Iceland-East is on the right (from Senior et al (2002)).

They used two Iceland SuperDARN HF radars to show the strong nightside convection activity during these quiet periods.

3.2 Tail reconnection during IMF northward non-substorm intervals (TRINNIs)

Milan et al (2005) observed similar flow bursts while studying transpolar arcs using auroral snapshots. The IMF conditions were northward, with B_z approximately 10 nT and B_y varied between -10 and +10 nT, no evidence of substorms was observed, but the conditions were not quiet according to the Gussenhoven (1998) criteria. In their study they considered the relative importance of B_y or B_z control. In these flow bursts, they found that reconnection bursts are an important component of the flux transfer mechanism within the magnetosphere and they coined the phrase "tail reconnection during IMF northward non-substorm intervals" to describe the phenomenon. The ionospheric convection measurements made by the SuperDARN radars are shown in the Fig.3.2, superimposed on the IMAGE auroral observations.

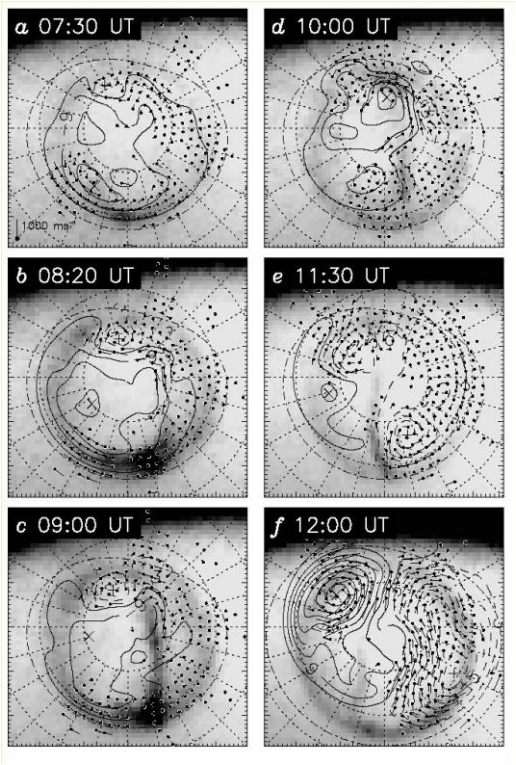

Fig. 3.2: Six (a – f) auroral snapshots, with SuperDARN estimates of the simultaneous ionospheric convection overlaid (from Milan et al (2005)).

The contours show the resulting potential pattern, solid and dashed contours for negative and positive potential, respectively, with a contour spacing of 6 kV. The vectors indicate the locations of radar observations that contributed to the potential solution and the length of these vectors is related to the flow speed.

3.3 Further observations of TRINNIs

A Series of observations were made by Grocott et al (2003, 2004, 2005, 2007) showing flow bursts, in some cases B_y controlling interhemispheric differences, where B_z varied between 5 and 10 nT and B_y varied between 5 and -10 nT. The IMF was consistently northward, but dominated by a significant B_y component, and no substorm activity was observed during these intervals.

(a)

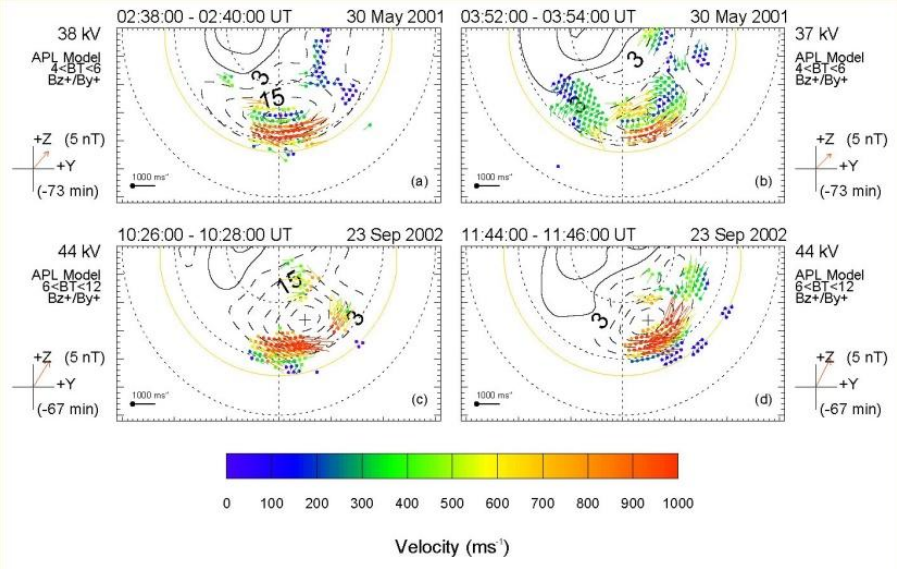

Fig. 3.3 (a): Flow maps illustrating the flow bursts from IMF northward intervals for northern hemisphere (from Grocott et al (2004)).

The above images show four bursts for the case of B_z positive and B_y positive. The velocity was greater than 1000 m/s during these flow bursts, which lasted about 10 minutes, dropping to lower values in between.

Simultaneous observations of magnetospheric flows by CLUSTER satellites were consistent with tail reconnection (Grocott et al., 2007). The SuperDARN radars observed the convection patterns in both hemispheres consistent with the IMF clock angle. They also observed similar localized bursts of flow in both hemispheres, as shown, for example, in Fig. 3.3(b). The coloured circles show the location of CLUSTER spacecraft during the period of interest. The colour coding for the CLUSTER data is red (C_2), green (C_3) and blue (C_4).

(b)

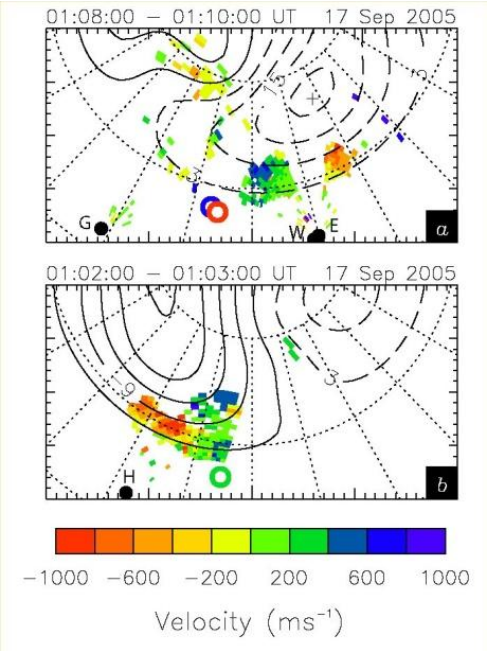

Fig. 3.3 (b): SuperDARN line-of-sight velocity from the northern hemisphere Iceland East (E), Iceland West (W), and Goose Bay (G) radars (upper panel) and the southern hemisphere Halley (H) radar (lower panel) (from Grocott et al (2007)).

CHAPTER 4

RESULTS

Figures 4.1 and 4.2 present data from the ACE spacecraft, from 01:40 to 03:40 UT for interval 1 on the 07 April 2006, lagged by 54 min, and from 20:30 to 22:30 UT for interval 2 on the 13 April 2006, lagged by 30 min. These extended intervals show the bulk speed of the solar wind and interplanetary magnetic field (IMF) for 30 minutes on either side of each interval of specific interest, namely from 02:10 to 03:10 UT for interval 1 and from 21:00 to 22:00 UT for interval 2, which is highlighted by the vertical solid lines. The IMF conditions are in GSM (geocentric solar magnetic) coordinates.

4.1 IMF and solar wind conditions

4.1.1 Interval 1: 07 April 2006 (02:10 – 03:10 UT)

In Fig. 4.1(a) the B_x, B_y, and B_z components of the IMF measured on the ACE spacecraft are shown. The B_x (-2,5 nT) is negative and the B_y (1,5 nT) and the B_z (0,5 nT) are both positive, but the B_y -component is stronger than the B_z -component throughout the interval. This means that the interval is one of northward, but with B_y dominating over the B_z -component of the IMF, which is consistent with the observed convection patterns and the orientation of the tail reconnection during IMF northward non-substorm interval (TRINNI) flows. The orientation of TRINNI flows depends on the IMF B_y as well as interhemispheric asymmetry, which has led several authors (including Nishida et al., 1995, 1998; Grocott et al., 2004, 2005) to suggest a mechanism for their generation based on the idea of magnetic field reconfiguration following reconnection in the twisted tail. The B_x -component of the IMF is negative, which is believed to favour northern hemisphere high-latitude reconnection. In Fig. 4.1(b), the solar wind bulk speed had become stable during the period of interest in this interval in the range (366 – 372 km/s). Thus during interval 1, the solar wind and geomagnetic activity were quiet according to Gussenhoven (1998) criteria for quite conditions (< 400 km/s, B_z < 2 nT and B < 5 nT).

(a) Interplanetary Magnetic Field Components

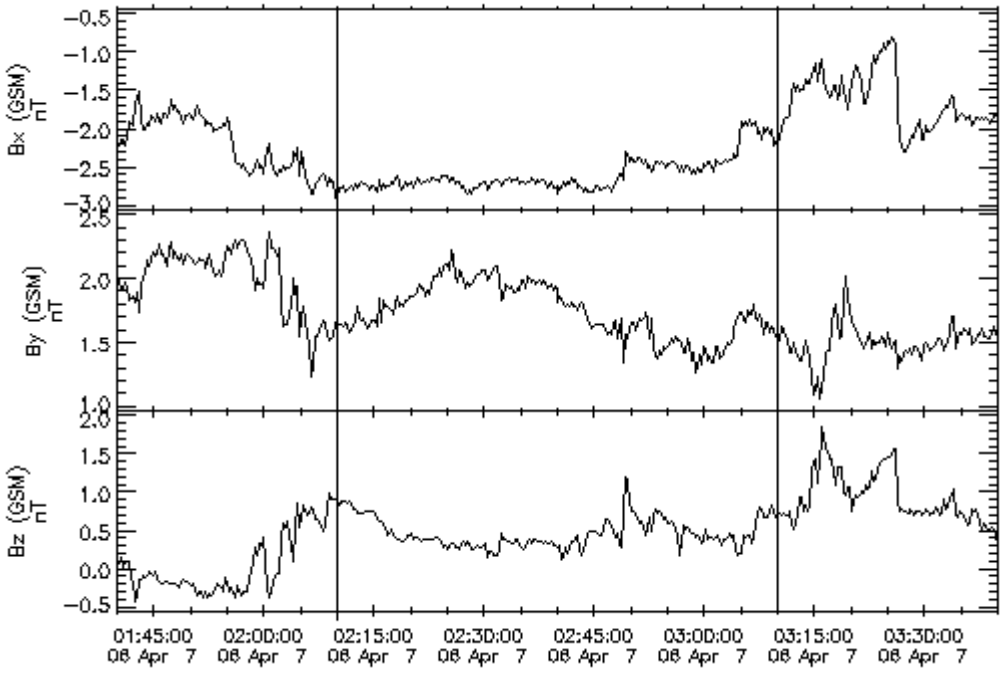

UT Time

(b) Solar Wind Bulk Speed

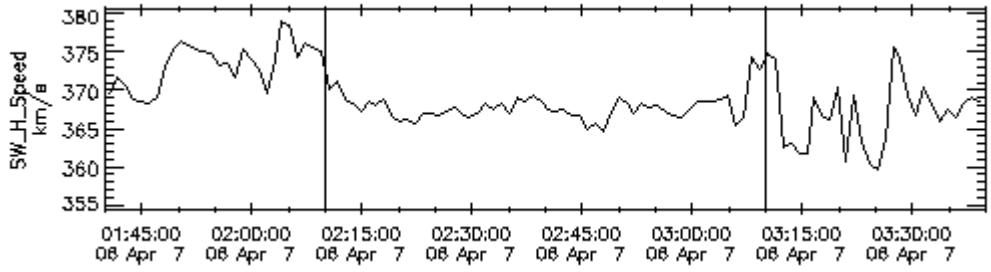

UT Time

Fig. 4.1: Upstream interplanetary observations from ACE spacecraft during 01:40 – 03:40 UT on 07 April 2006, lagged by 54 min to account for the propagation delay to the magnetosphere (adapted from CDAWeb http://cdaweb.gsfc.nasa.gov/).

4.1.2 Interval 2: 13 April 2006 (21:00 – 22:00 UT)

In Fig. 4.2(a), all three components of the IMF measured on the ACE spacecraft are shown. The B_x (3.5 nT) and B_z (4 nT) components of the IMF are both positive but B_y (-16.5 nT) is strongly negative throughout the interval. This means that the interval is one of northward, but negative B_y -dominated IMF, which is consistent with the observed convection patterns and the orientation of the tail reconnection during IMF northward non-substorm interval flows. The B_x -component of the IMF is positive which is believed to favour southern hemisphere high-latitude reconnection (Lockwood & Moen, 1999; Hu et al., 2006). The solar wind bulk speed is high at an average of about 520 km/s shown in Fig. 4.3(b) for this interval.

(a) Interplanetary Magnetic Field components

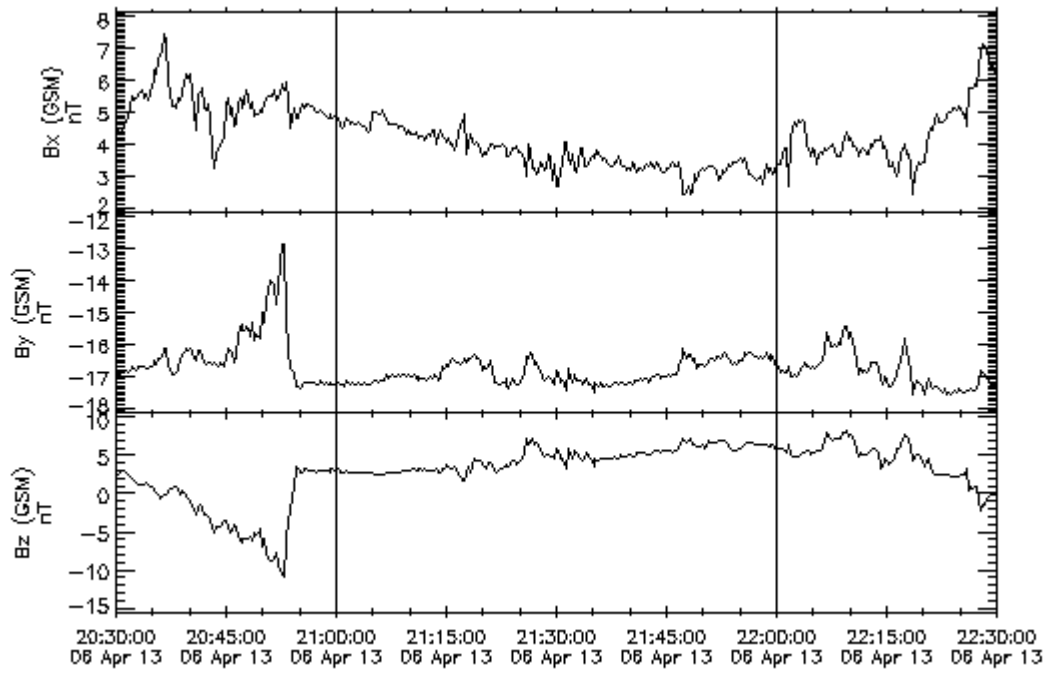

UT Time

(b) Solar Wind Bulk Speed

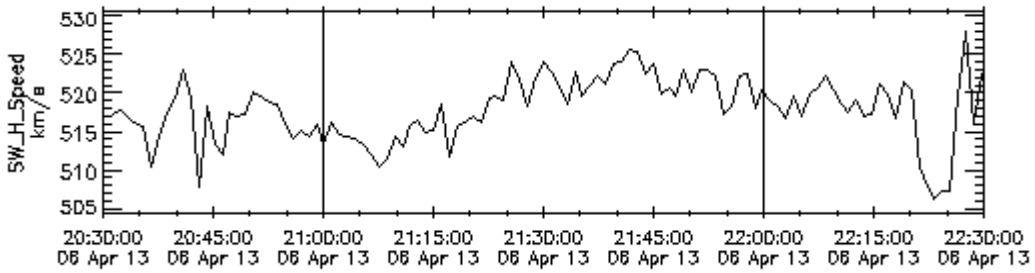

Fig. 4.2: Upstream interplanetary observations from ACE spacecraft during 20:30 – 22:30 UT on 13 April 2006 lagged by 30 min to account for the propagation delay to the magnetosphere (adapted from CDAWeb http://cdaweb.gsfc.nasa.gov/).

4.2 Convection patterns and effect of B_y

Figure 4.3 shows the convection maps of the ionospheric flow observed by the SuperDARN radars. The dayside and nightside ionosphere of the globe are indicated by the absence of shading and grey shading, respectively. The origin of the plasma irregularities detected by the SuperDARN radars is indicated by the dots and the tails point in the direction of the bulk velocity. The solid and dashed contours represent the paths of the plasma circulation. The green line is called the Heppner-Maynard boundary and characterizes the size of the convection zone. The flow vectors are colour coded according to the velocity colour bar indicated on the left, with the vector length scale also being indicated in the top left of the globe. The 'x' and '+' represent the locations of the extreme potential values and the difference between these two extremes gives the total cross polar cap potential (CPCP). The inset in the top right of each map shows the orientation of the IMF in the YZ GSM plane.

Fig. 4.3: Ionospheric convection maps of the (a) northern hemisphere and (b) southern hemisphere, observed by the SuperDARN radars when the interval was characterized by $B_z > 0$.

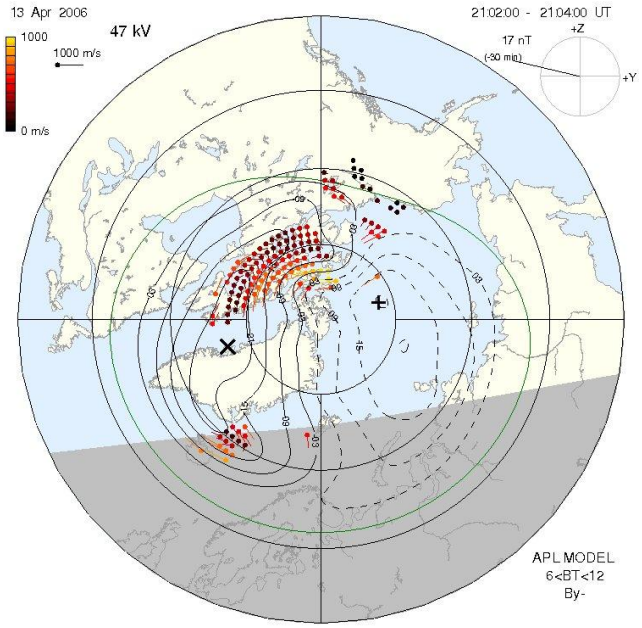

(a) Northern hemisphere convection map

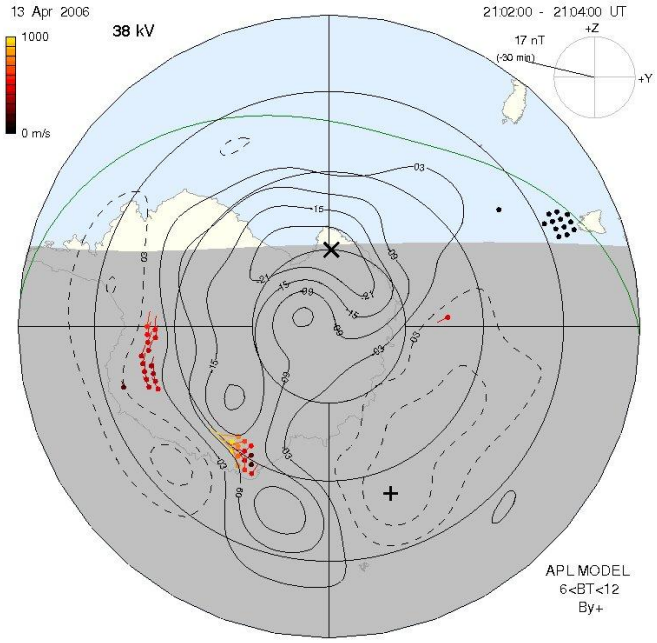

(b) Southern hemisphere convection map

These convection maps were observed in an interval with $B_z > 0$, where B_y was strongly dominating B_z. The ionospheric convection pattern is much more structured than is the case for $B_z > 0$ with small B_y, confined to much higher latitudes involving flow driven by reconnection between the IMF and the open field lines of the magnetotail. The presence of a strong B_y component of the IMF creates asymmetry in the dawn-dusk direction. This shows that the convection patterns depend on the orientation of the B_y -component of the IMF.

4.3 Flow bursts in both hemispheres simultaneously

Figs. 4.4 and 4.5 show four pairs of convection maps of the nightside ionosphere high-latitude flow observed by the SuperDARN radars. The flow bursts were observed during geomagnetic quiet periods, with northward IMF, but B_y was dominating the B_z -component of the IMF throughout the interval.

4.3.1 Interval 1: 07 April 2006 (02:10 – 03:10 UT)

In Fig. 4.4, panels (a), (c), (e) and (g) show the northern hemisphere flows when B_y was positive. The dominant flow feature is a < 1000 m/s westward burst in the nightside ionosphere for each case. In this interval the convection patterns are well defined. There are also localized areas of high speed flow ~1000 m/s on the nightside, directed westward (excluding panel (e)). Panels (b), (d), (f) and (h) show the southern hemisphere flow. The convection patterns are well defined. They have similar flow features, with a < 1000 m/s eastward burst in the nightside ionosphere. In panel (f), there is a localized area of similar high speed flow for the westward burst on the dayside ionosphere.

Fig. 4.4: The nightside ionospheric flow derived from SuperDARN velocity measurements. These maps were generated at the University of KwaZulu-Natal (SHARE computer lab) using Radar Software Toolkit (RST).

(a)

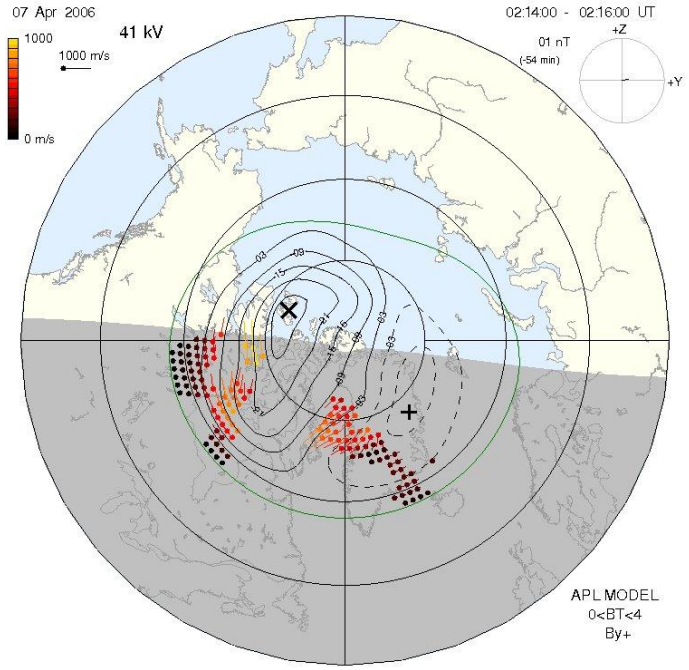

(b)

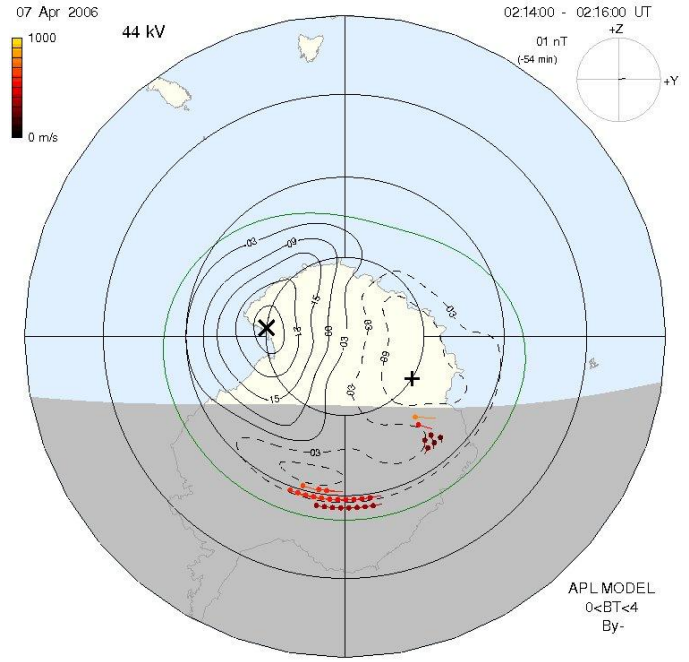

(c)

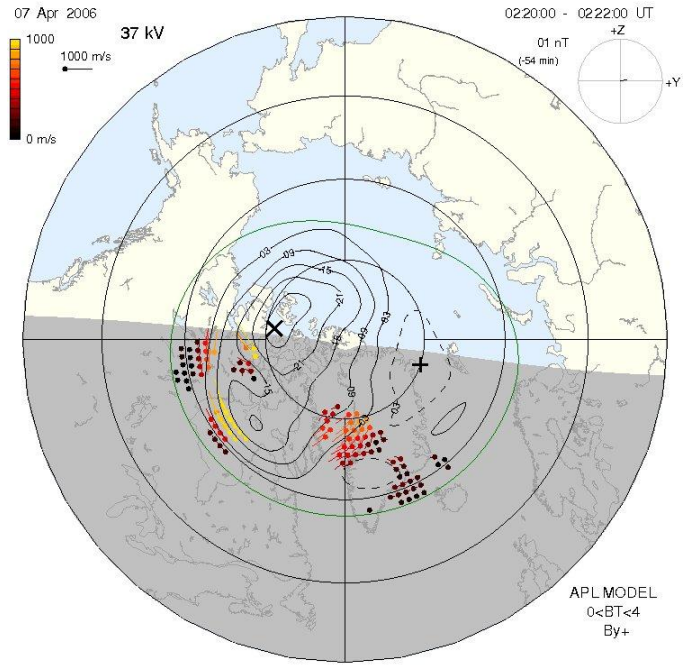
07 Apr 2006
37 kV
1000
1000 m/s
0 m/s
0220:00 - 0222:00 UT
01 nT
(-54 min)
+Z
+Y
APL MODEL
0<BT<4
By+

(d)

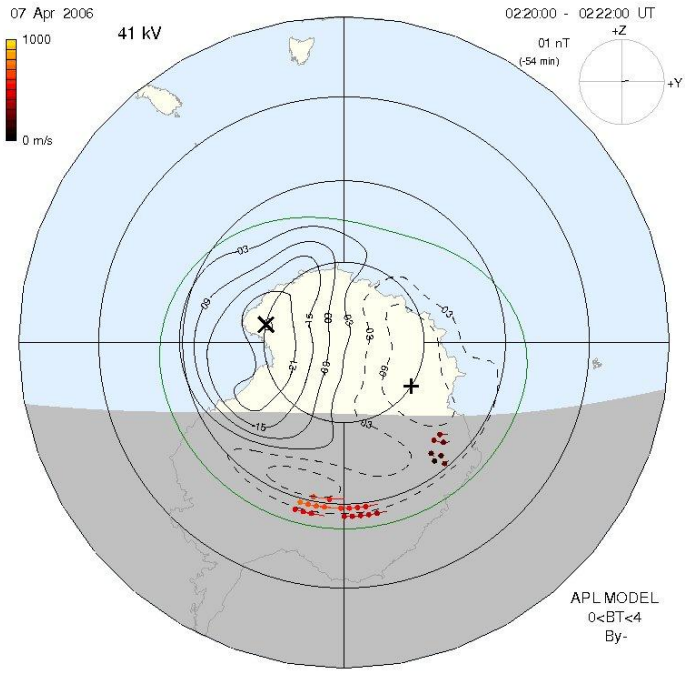
07 Apr 2006
41 kV
1000
0 m/s
0220:00 - 0222:00 UT
01 nT
(-54 min)
+Z
+Y
APL MODEL
0<BT<4
By-

(e)

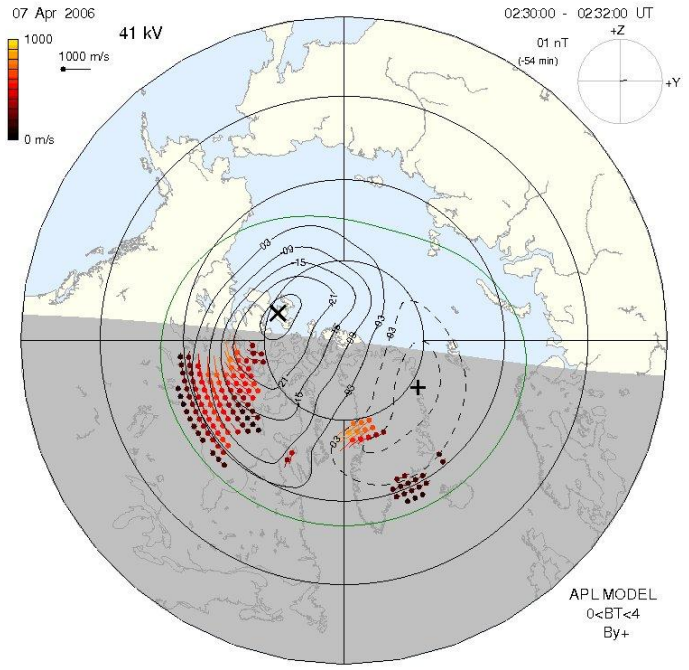
07 Apr 2006
41 kV
1000
1000 m/s
0 m/s
02:30:00 - 02:32:00 UT
+Z
01 nT
(-54 min)
+Y
APL MODEL
0<BT<4
By+

(f)

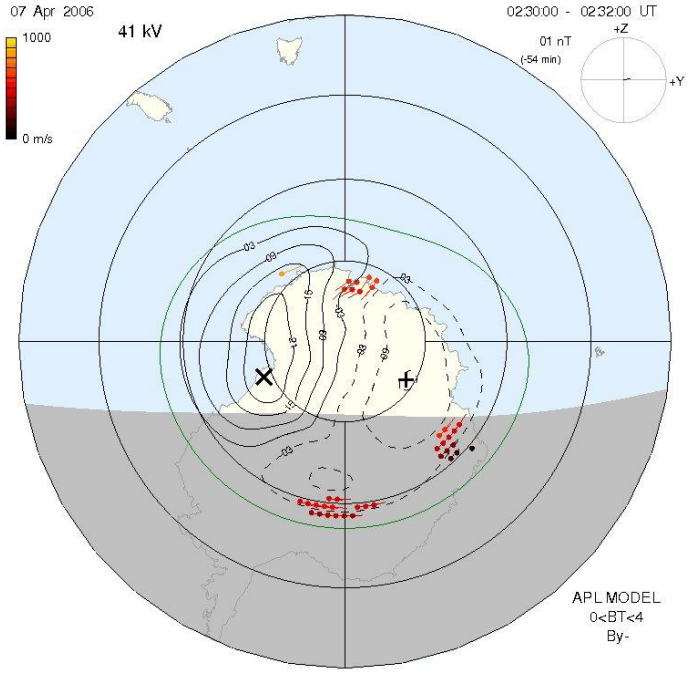
07 Apr 2006
41 kV
1000
0 m/s
02:30:00 - 02:32:00 UT
+Z
01 nT
(-54 min)
+Y
APL MODEL
0<BT<4
By-

(g)

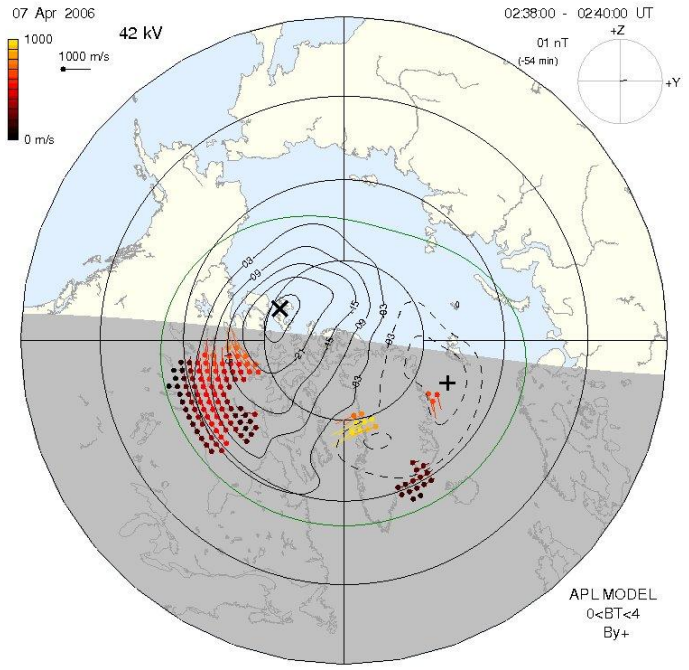
07 Apr 2006
42 kV
1000
1000 m/s
0 m/s
02:38:00 - 02:40:00 UT
+Z
01 nT
(-54 min)
+Y
APL MODEL
0<BT<4
By+

(h)

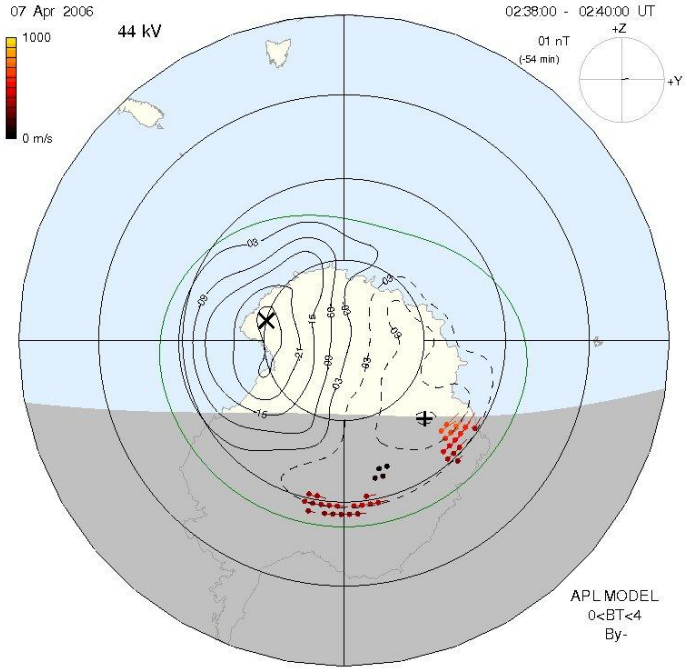
07 Apr 2006
44 kV
1000
0 m/s
02:38:00 - 02:40:00 UT
+Z
01 nT
(-54 min)
+Y
APL MODEL
0<BT<4
By-

4.3.2 Interval 2: 13 April 2006 (21:00 – 22:00 UT)

In Fig. 4.5, panels (a), (c), (e) and (g) show the northern hemisphere flow when B_y was strongly negative. In the dayside ionosphere, the dominant flow feature is a ~1000 m/s westward burst for each interval, part of a well defined convection pattern. There are also localized areas of high speed flow < 1000 m/s in the nightside ionosphere, directed westward. Panels (b), (d), (f) and (h) show the southern hemisphere flow: there are no clear convection patterns, but there are similar dominant flow features with a ~1000 m/s westward flow burst in the nightside ionosphere.

Fig. 4.5: The nightside ionospheric flow derived from SuperDARN velocity measurements. These maps were generated at the University of KwaZulu-Natal (SHARE computer lab) using Radar Software Toolkit (RST).

(a)

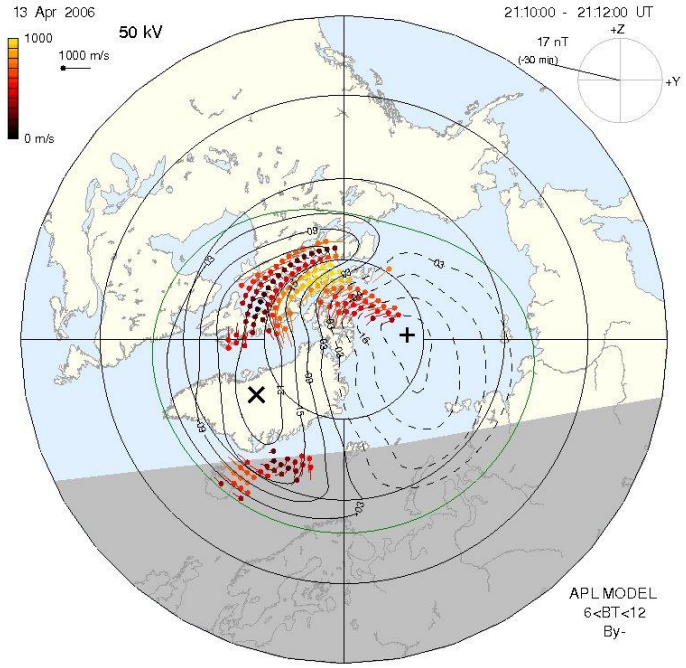

(b)

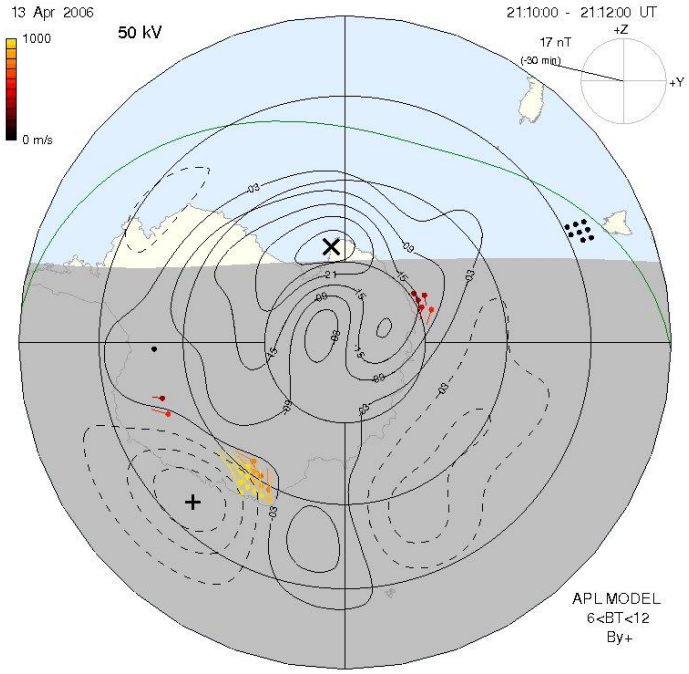

(c)

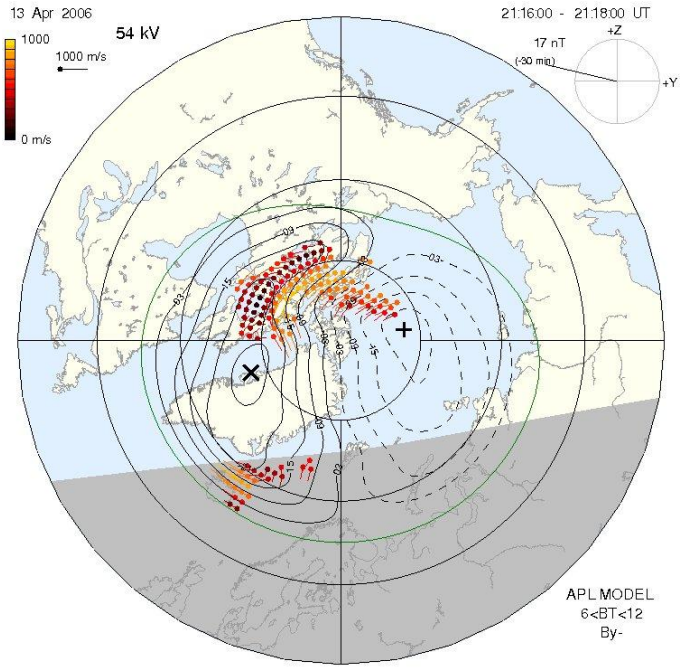
13 Apr 2006
54 kV
1000
1000 m/s
0 m/s
21:16:00 - 21:18:00 UT
17 nT
(-30 min)
+Z
+Y
APL MODEL
6<BT<12
By-

(d)

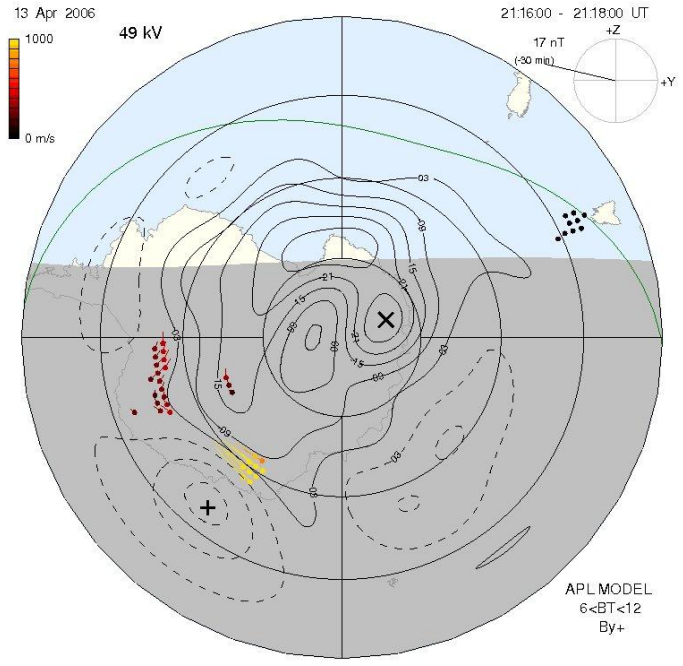
13 Apr 2006
49 kV
1000
0 m/s
21:16:00 - 21:18:00 UT
17 nT
(-30 min)
+Z
+Y
APL MODEL
6<BT<12
By+

(e)

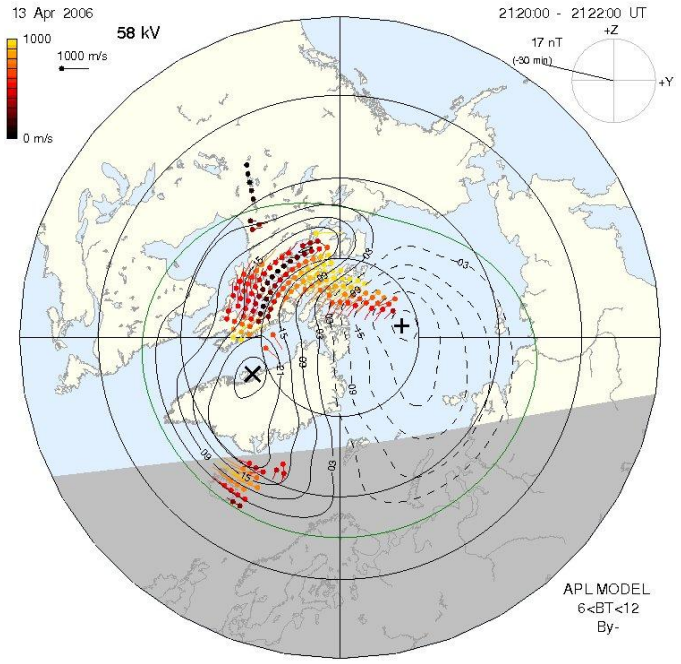
13 Apr 2006
58 kV
1000
1000 m/s
0 m/s
2120:00 - 2122:00 UT
17 nT
(-30 min)
+Z
+Y
APL MODEL
6<BT<12
By-

(f)

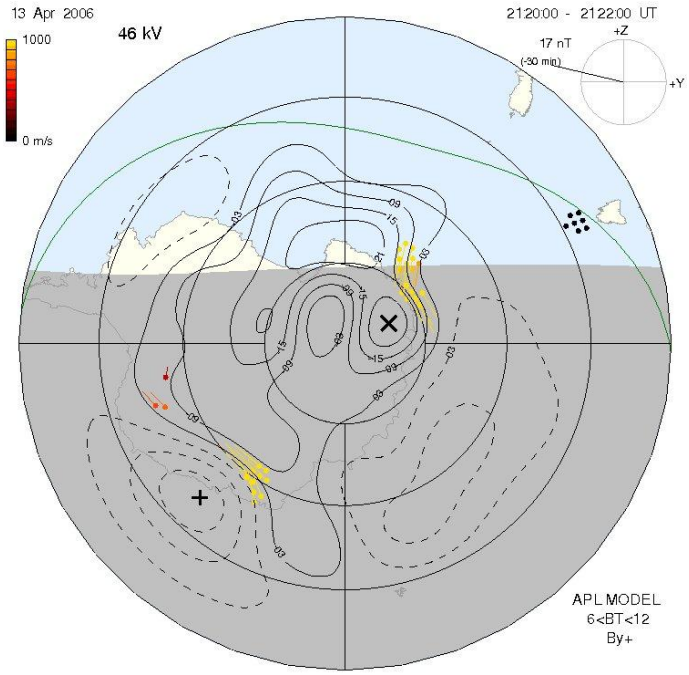
13 Apr 2006
46 kV
1000
0 m/s
2120:00 - 2122:00 UT
17 nT
(-30 min)
+Z
+Y
APL MODEL
6<BT<12
By+

(g)

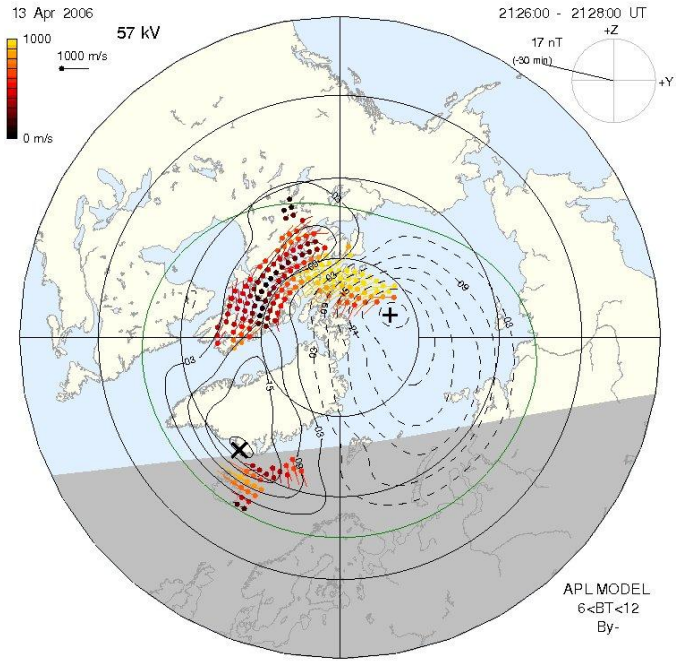
13 Apr 2006
57 kV
1000
1000 m/s
0 m/s
2126:00 - 2128:00 UT
17 nT
(-30 min)
+Z
+Y
APL MODEL
6<BT<12
By-

(h)

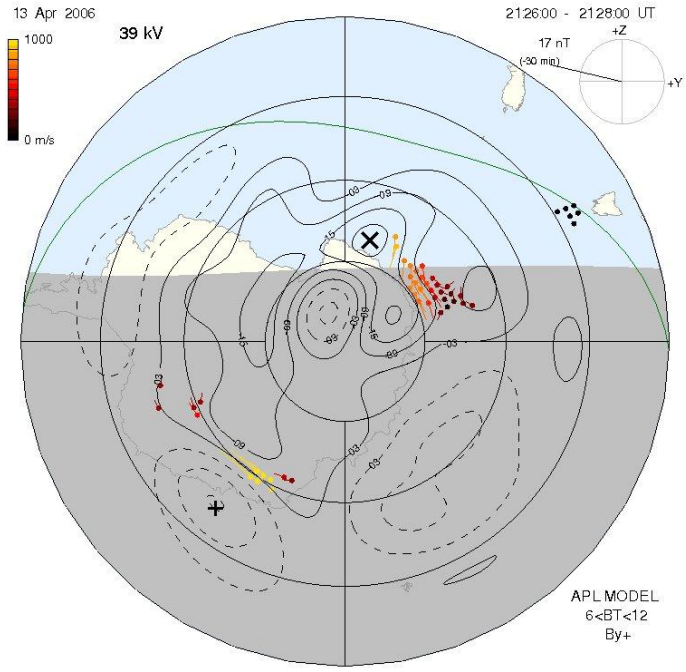
13 Apr 2006
39 kV
1000
0 m/s
2126:00 - 2128:00 UT
17 nT
(-30 min)
+Z
+Y
APL MODEL
6<BT<12
By+

4.4 Radar field of view

Figs. 4.6 and 4.7 show the field of view of the SuperDARN radars in interval 1 and interval 2. The colour regions depict F -region irregularities moving with the bulk plasma velocity. The blue colouring represents velocities moving toward the radar and the red -green colours represent velocities moving away from the radar. These radars will be discussed in more details on the time series plots below in Fig. 4.8 and 4.9. We have selected the following radars based on their better backscatter.

4.4.1 Interval 1: 07 April 2006 (02:10 - 03:10 UT)

Fig. 4.6: Field of view of the SuperDARN radars for interval 1 at the times shown on the plots, were generated at the University of KwaZulu-Natal (SHARE computer lab).

(a) Kapuskasing radar field of view

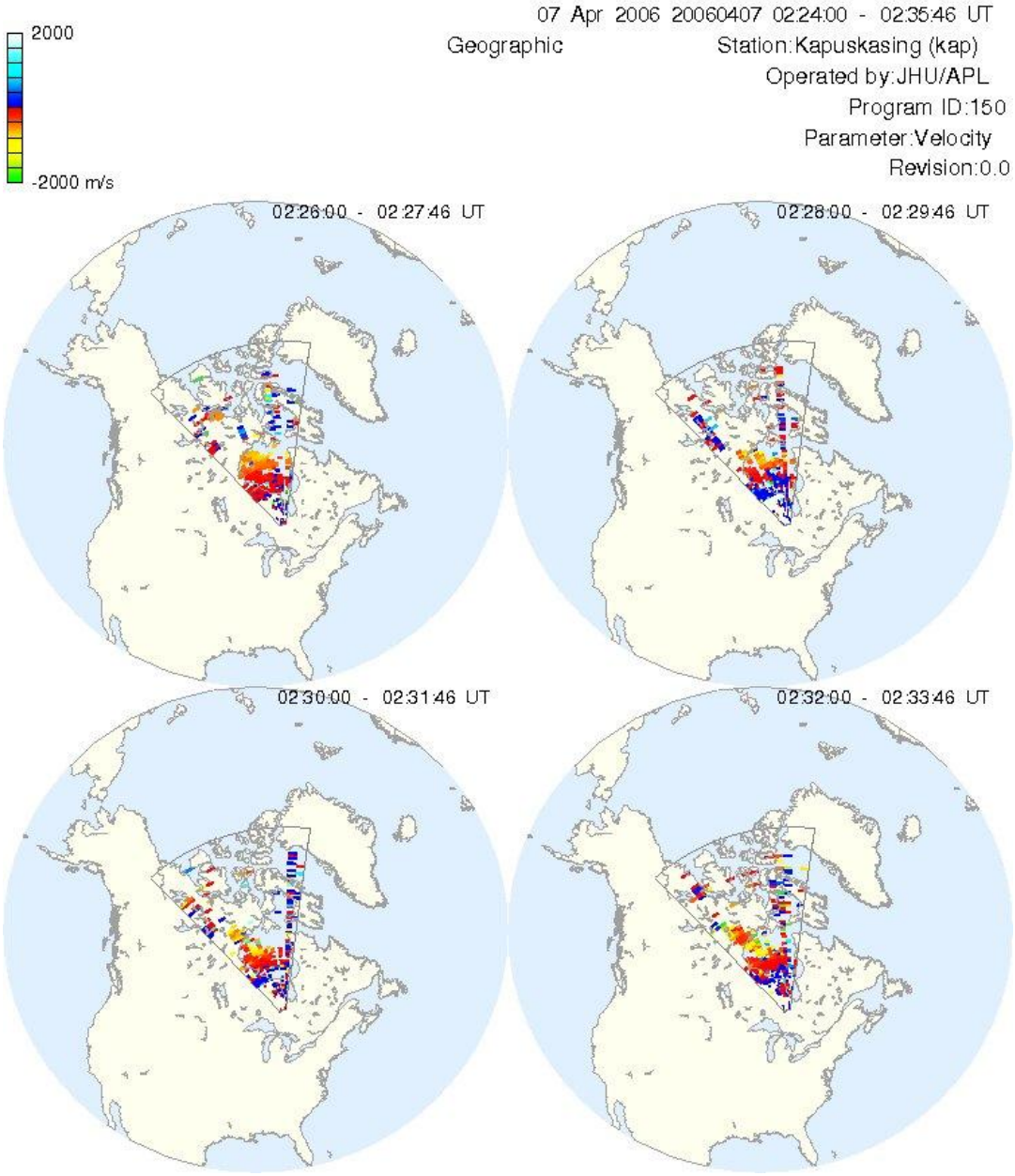

(b) Stokkseyri radar field of view

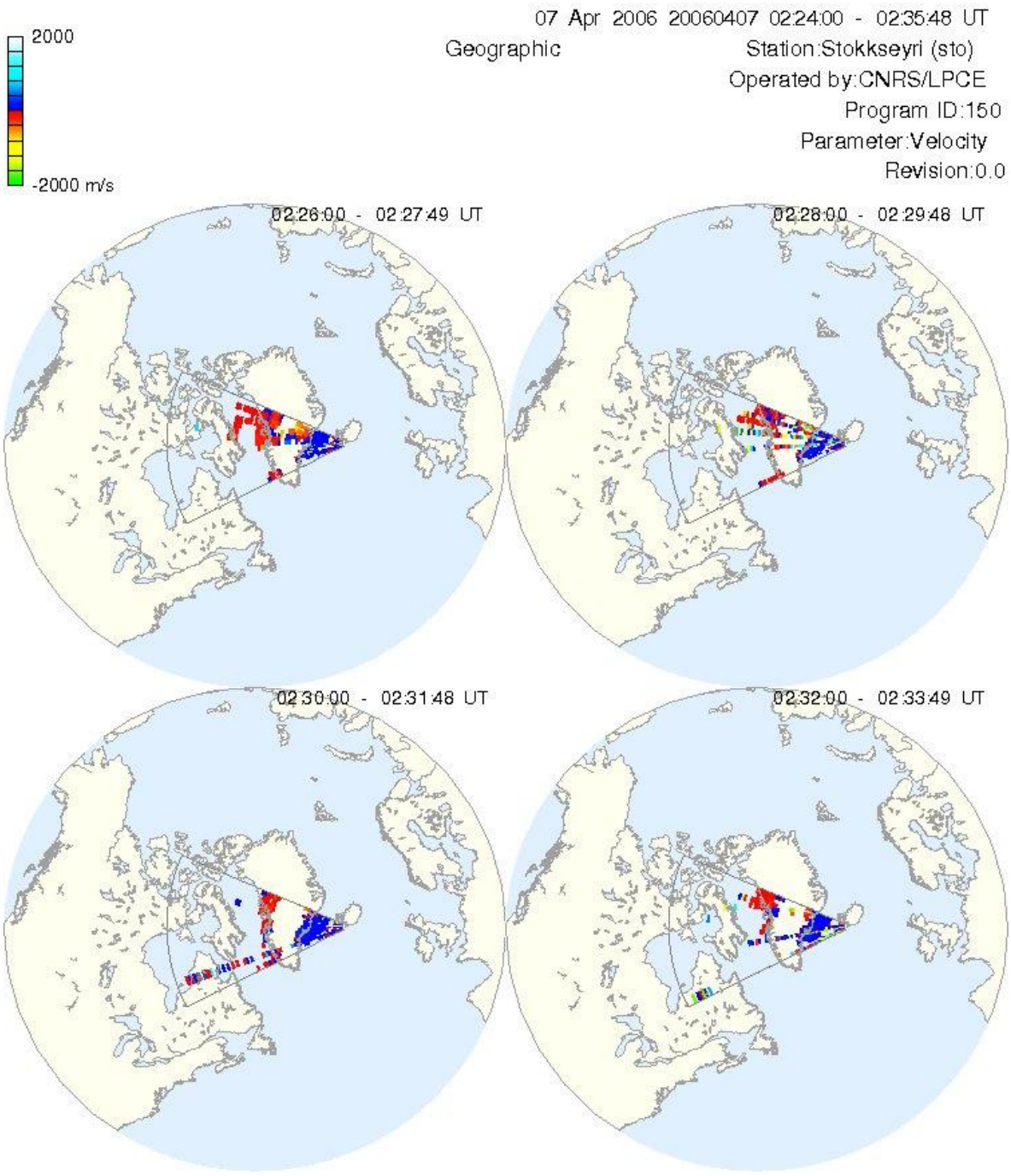

(c) Syowa East radar field of view

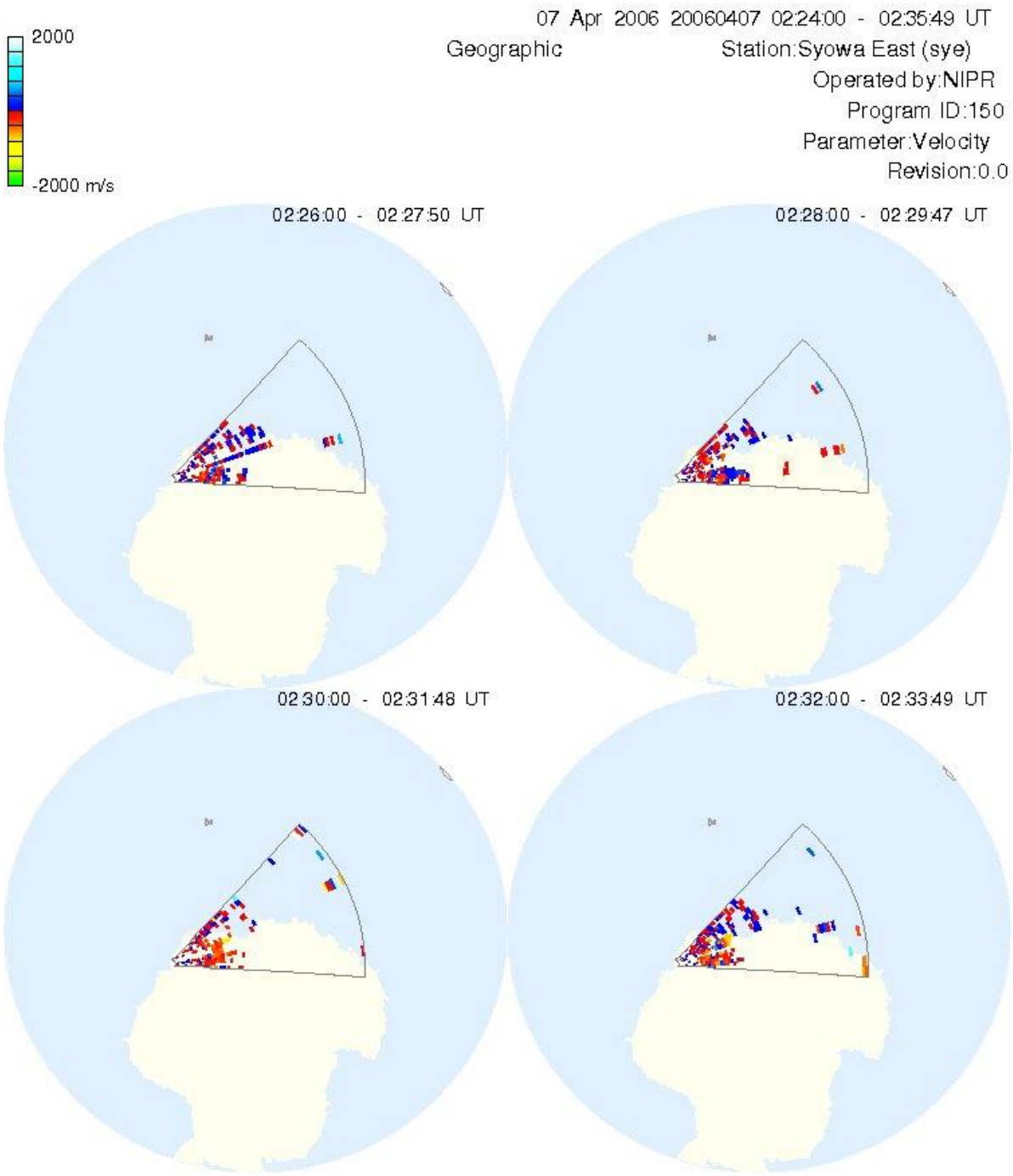

4.4.2 Interval 2: 13 April 2006 (21:00-22:00 UT)

Fig. 4.7: Field of views of the SuperDARN radars for interval 1 at the times shown on the plots, were generated at the University of KwaZulu-Natal (SHARE computer lab).

(a) Kodiak radar field of view

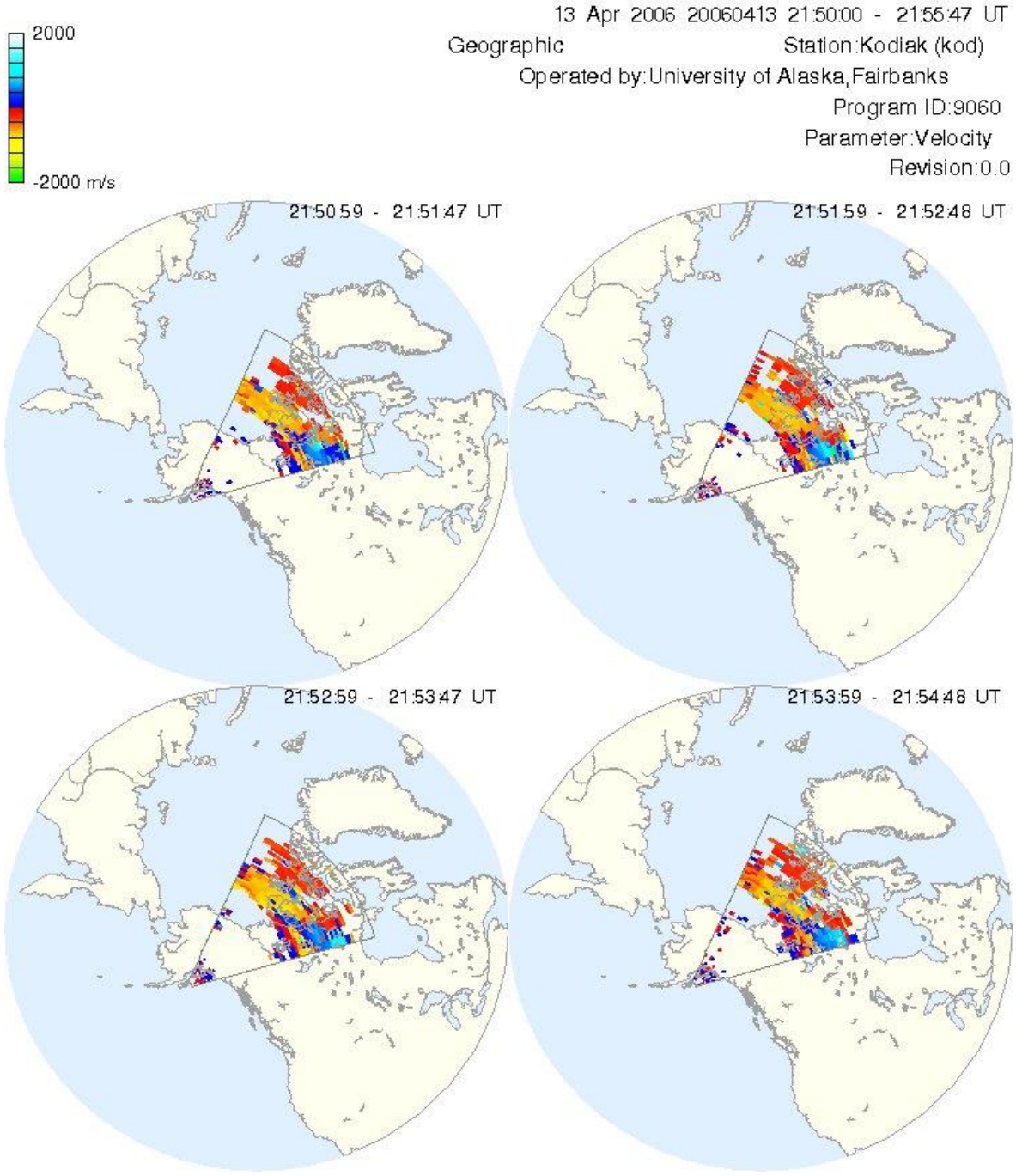

(b) Kapuskasing radar field of view

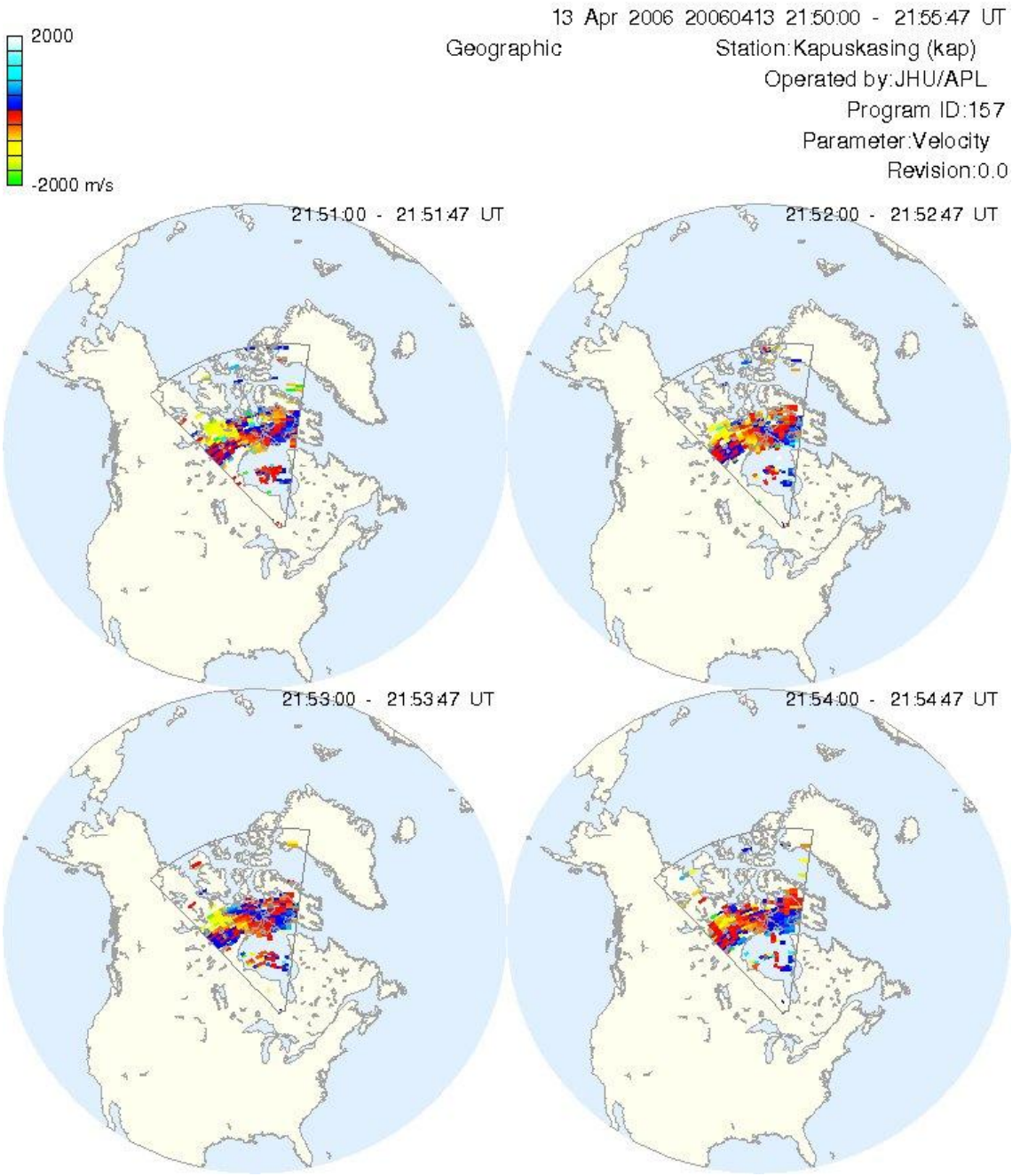

(c) Sanae radar field of view

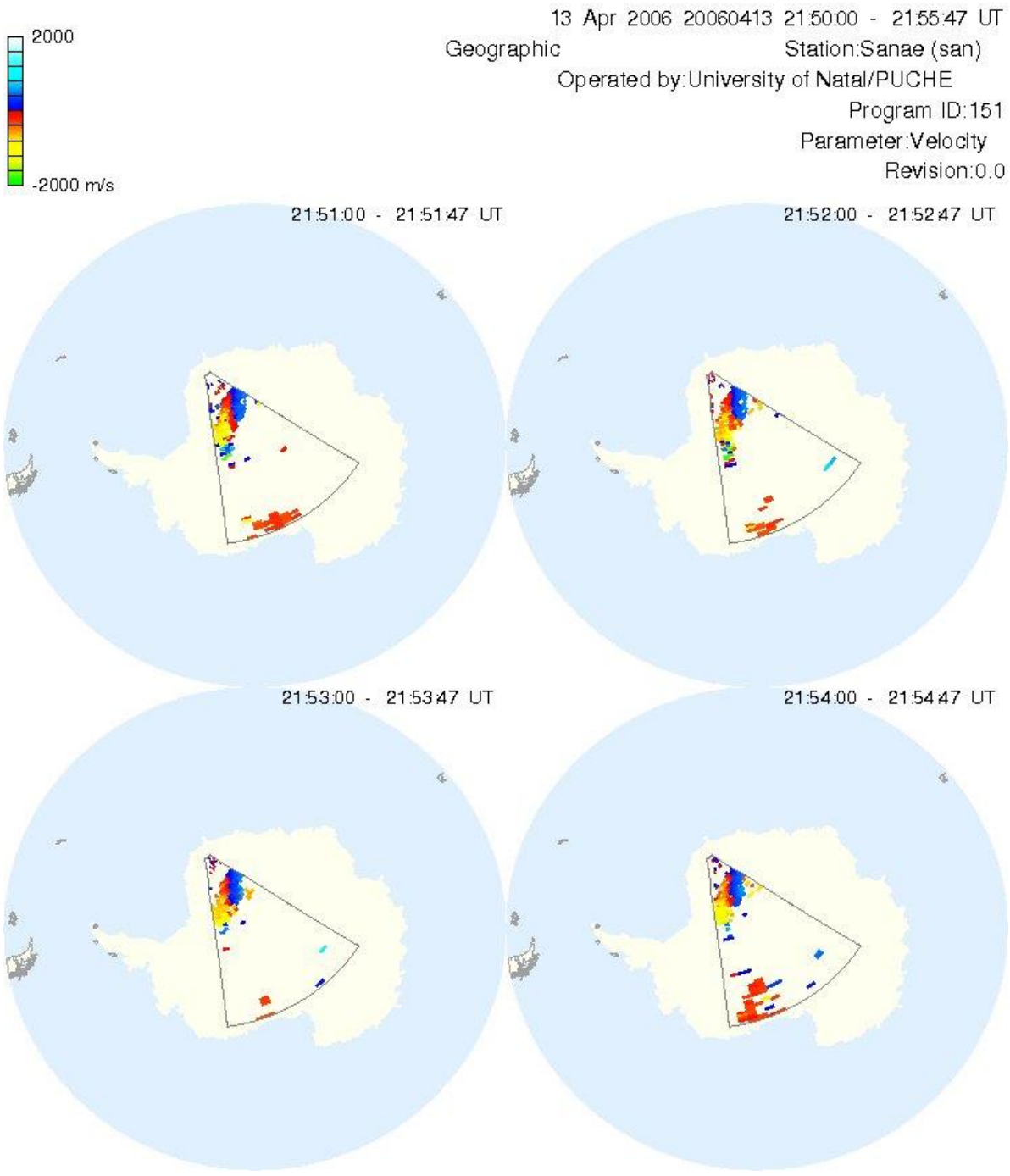

(d) Tiger radar field of view

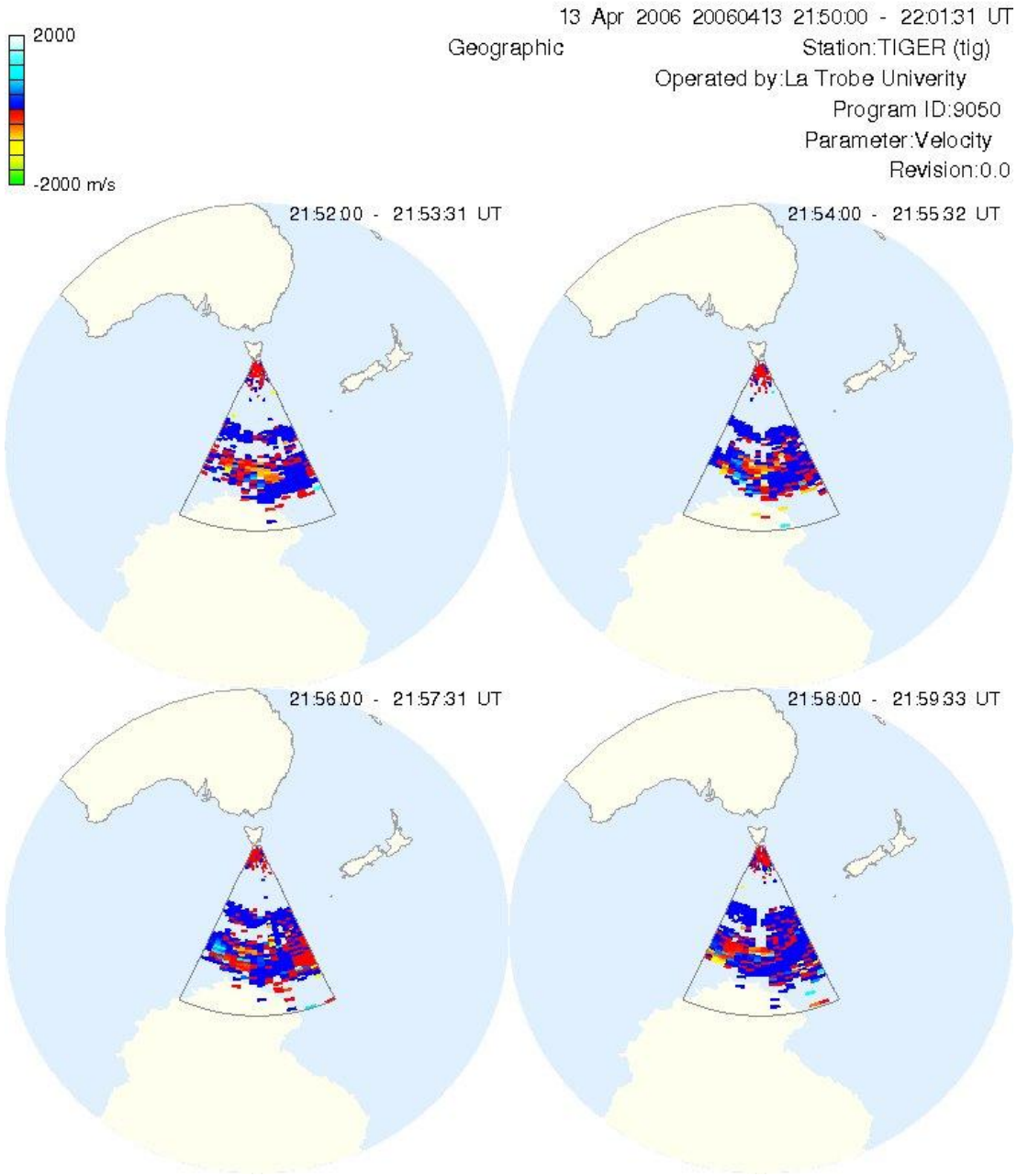

4.5 Time series plots

Figs. 4.8 and 4.9 show time series of parameters for each radar: from top to bottom are backscatter power, line of sight Doppler velocity and spectral width. The horizontal axis represents universal time (UT) while the vertical axes represent range gate. Each parameter is color-coded according to the color bars displayed on the right. In the middle panel, blue coloring indicates velocities moving toward the radar, while the red-green colors correspond to velocities away from the radar. Areas of grey shading identify velocity measurements that have been flagged as groundscatter, based on simultaneously low values of spectral width and velocity magnitude. At the top of the figure are color-coded time series of the transmitted frequency and the receiver. We have selected the following radars based on their better backscatter.

4.5.1 Interval 1 : 07 April 2006 (02:10 – 03:10 UT)

Fig. 4.8: Backscatter power, line-of-sight Doppler velocity and spectral width measured between 02:10 – 03:10 UT, were generated at the University of KwaZulu-Natal (SHARE computer lab).

(a) Kapuskasing radar from northern hemisphere

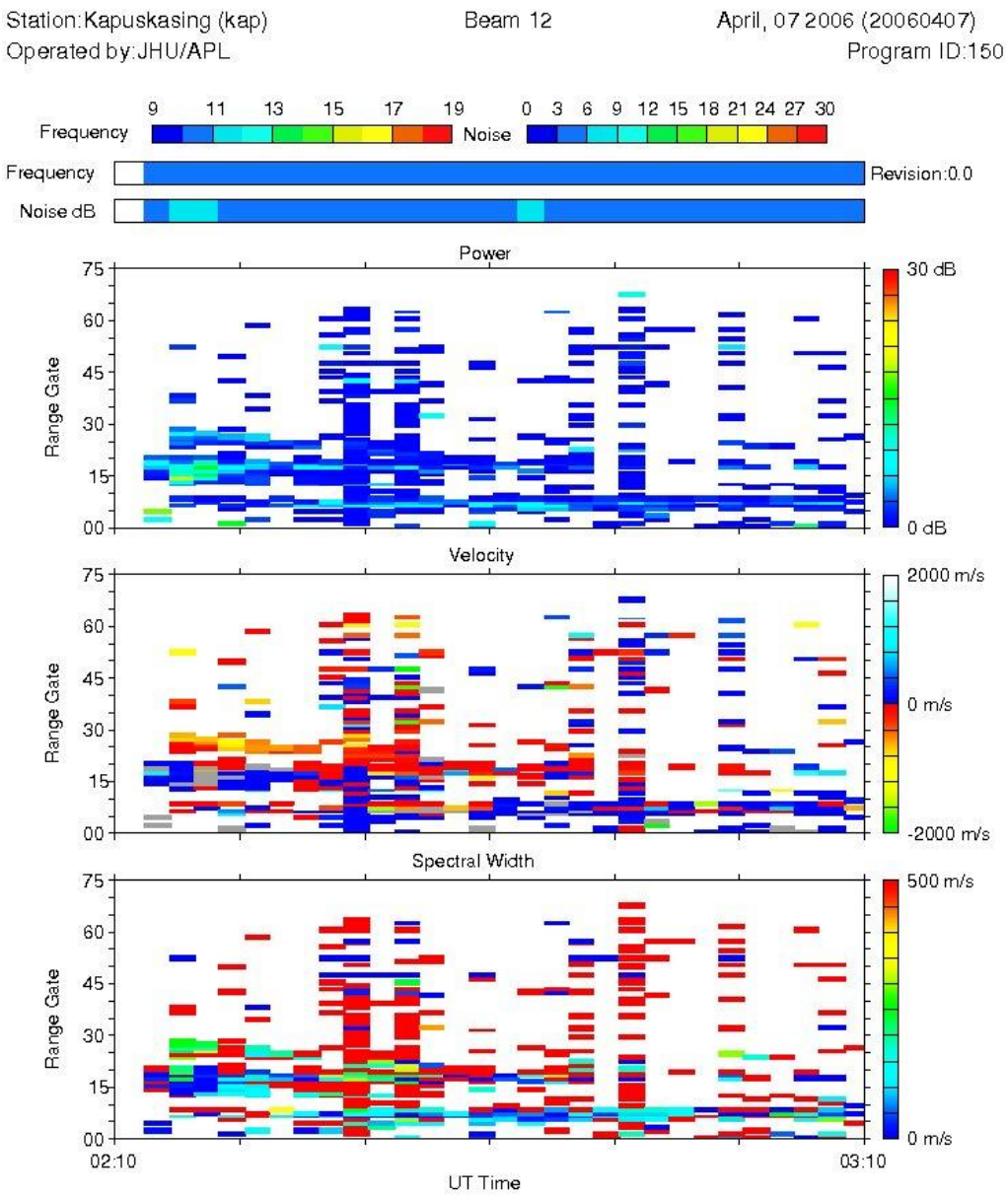

In the middle panel, the line-of-sight Doppler velocities are predominantly moving away from the radar, corresponding to anti-sunward flows, which are variable with time.

(b) Stokkseyri radar from northern hemisphere

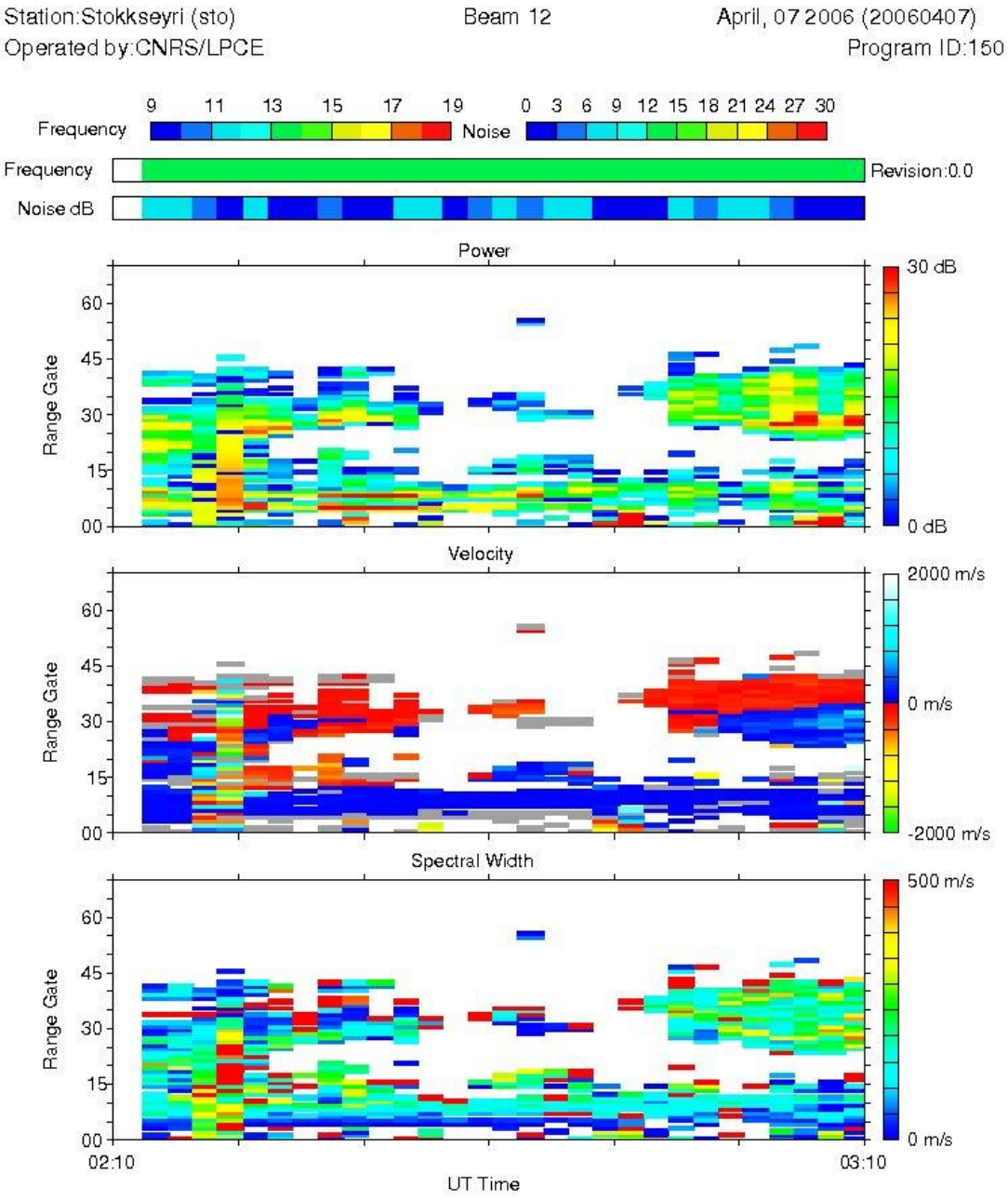

In the middle panel, the Doppler velocity is predominantly observing plasma flow moving toward the radar below the range gate 30, which corresponds to sunward flow. Above range gate 30 the line-of-sight Doppler velocity observes plasma flow moving away from the radar, corresponding to anti-sunward flow.

(c) Syowa East radar from southern hemisphere

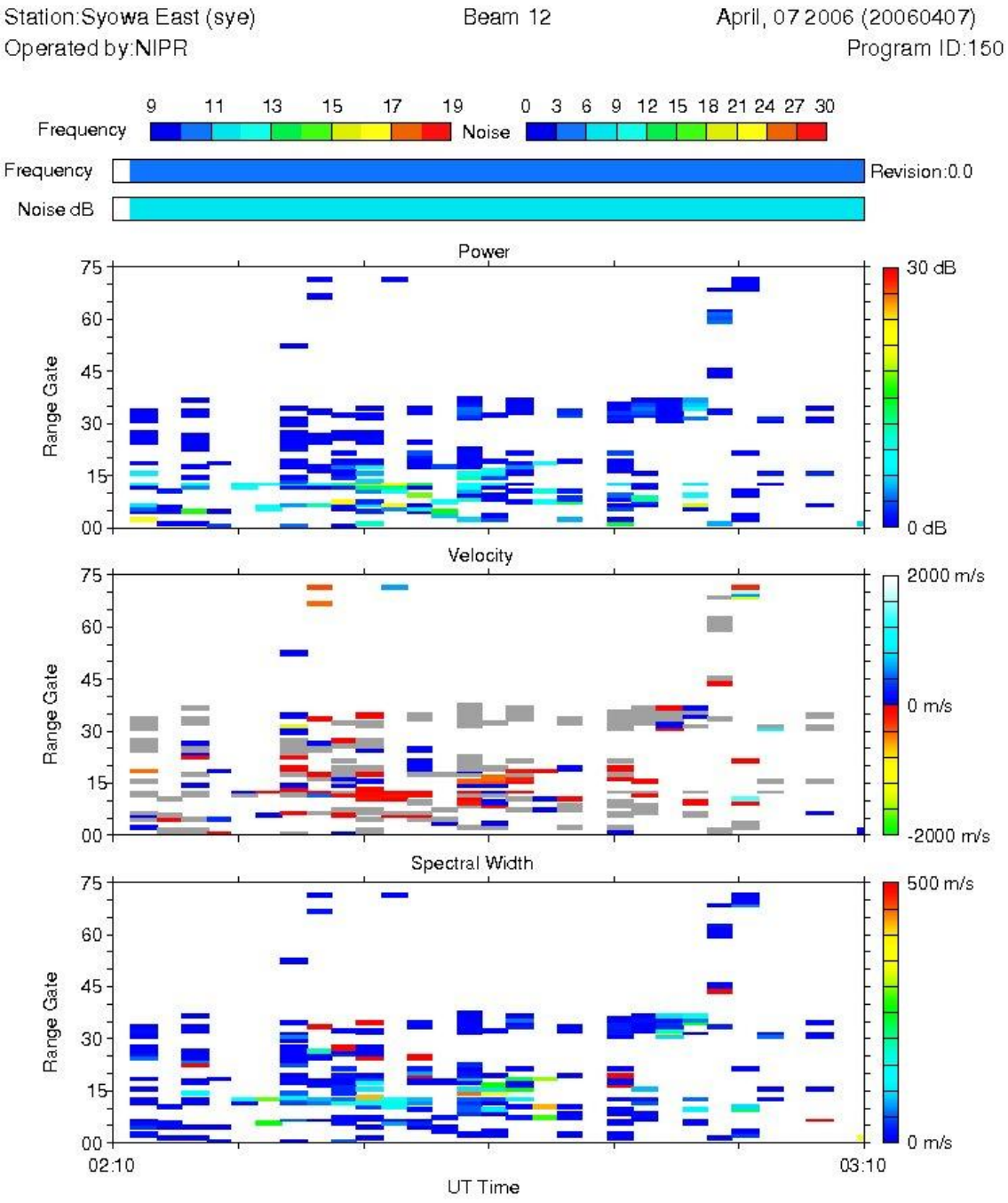

In the middle panel, the Syowa East radar is observing little backscatter throughout the interval.

4.5.2 Interval 2: Interval 2 : 13 April 2006 (21:00 – 22:00 UT)

Fig. 4.9: Backscatter power, line-of-sight Doppler velocity and spectral width measured between 21:00 – 22:00 UT, were generated at the University of KwaZulu-Natal (SHARE computer lab).

(a) Kodiak radar from northern hemisphere.

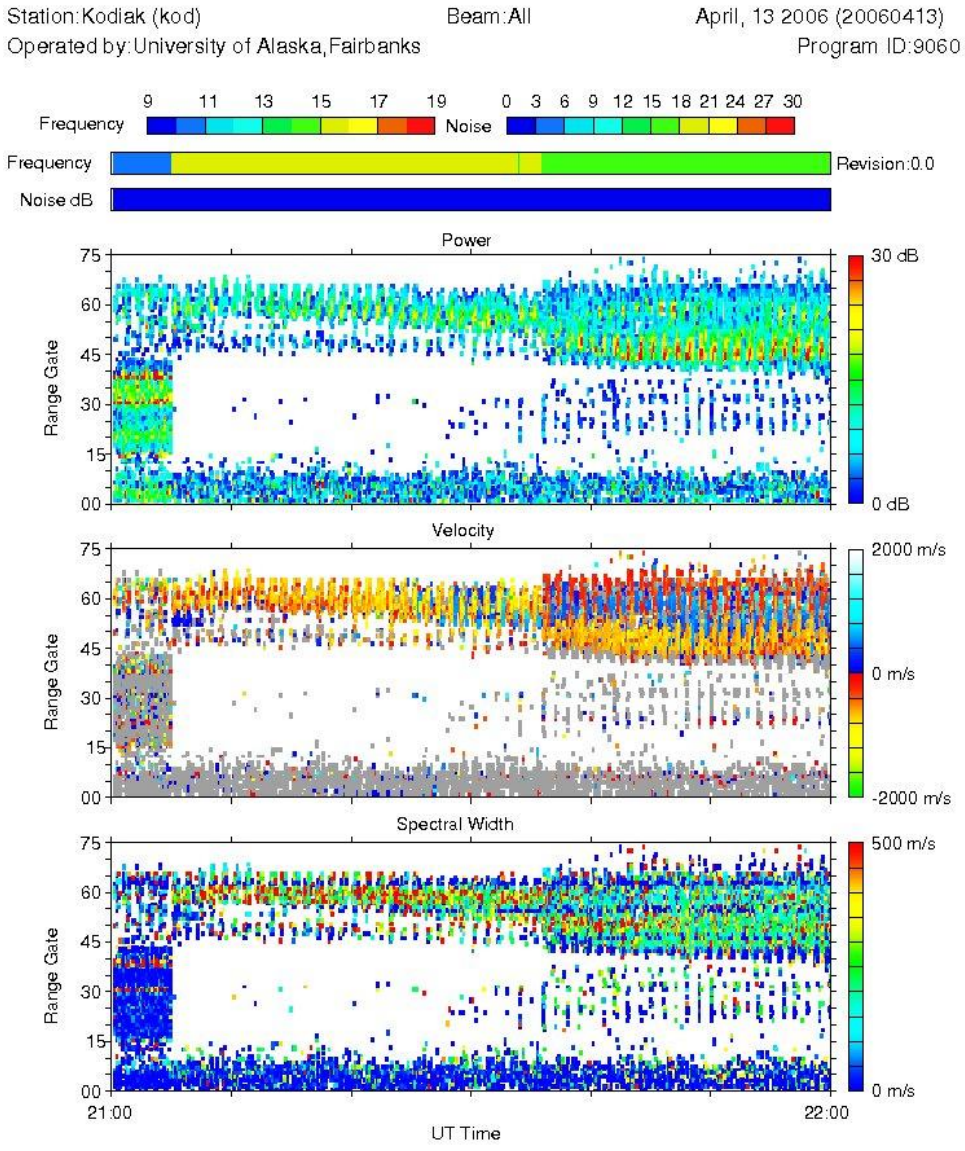

In the middle panel, the radar observed little scatter below range gate 45, and the Doppler velocities were predominantly moving away from the radar as from 21:00 to 21:05 UT.

Above range gate 45, the Kodiak radar observed fast plasma flow moving away from the radar from 21:00 to 21:35 UT, which corresponds to anti-sunward flow. From 21:35 to 22:00 UT, the Doppler velocity is predominantly away from the radar.

(b) Kapuskasing Radar from northern hemisphere

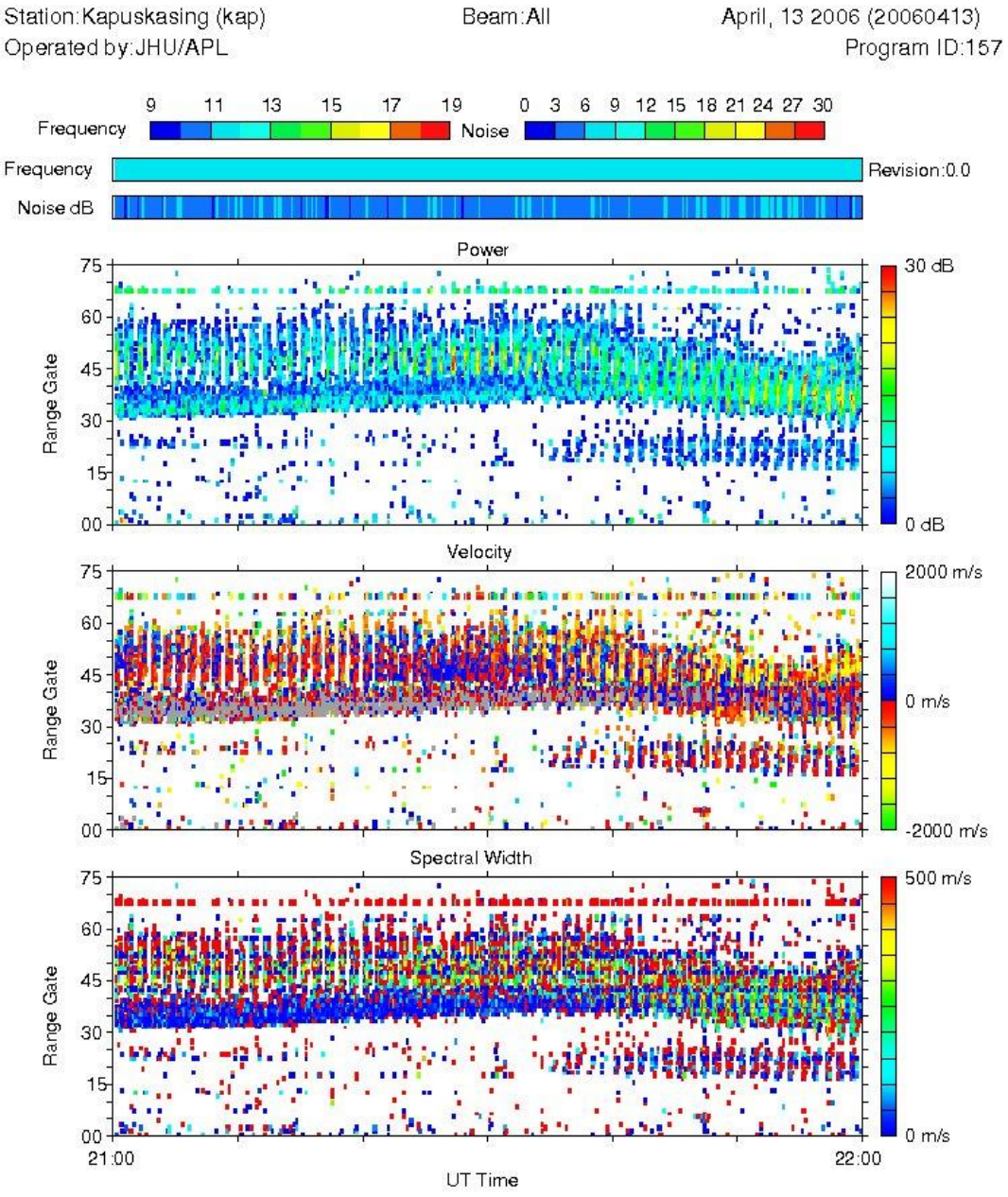

In the middle panel, the Kapuskasing radar observed strong plasma flow moving away from the radar, which is variable with time.

(c) Sanae radar from southern hemisphere

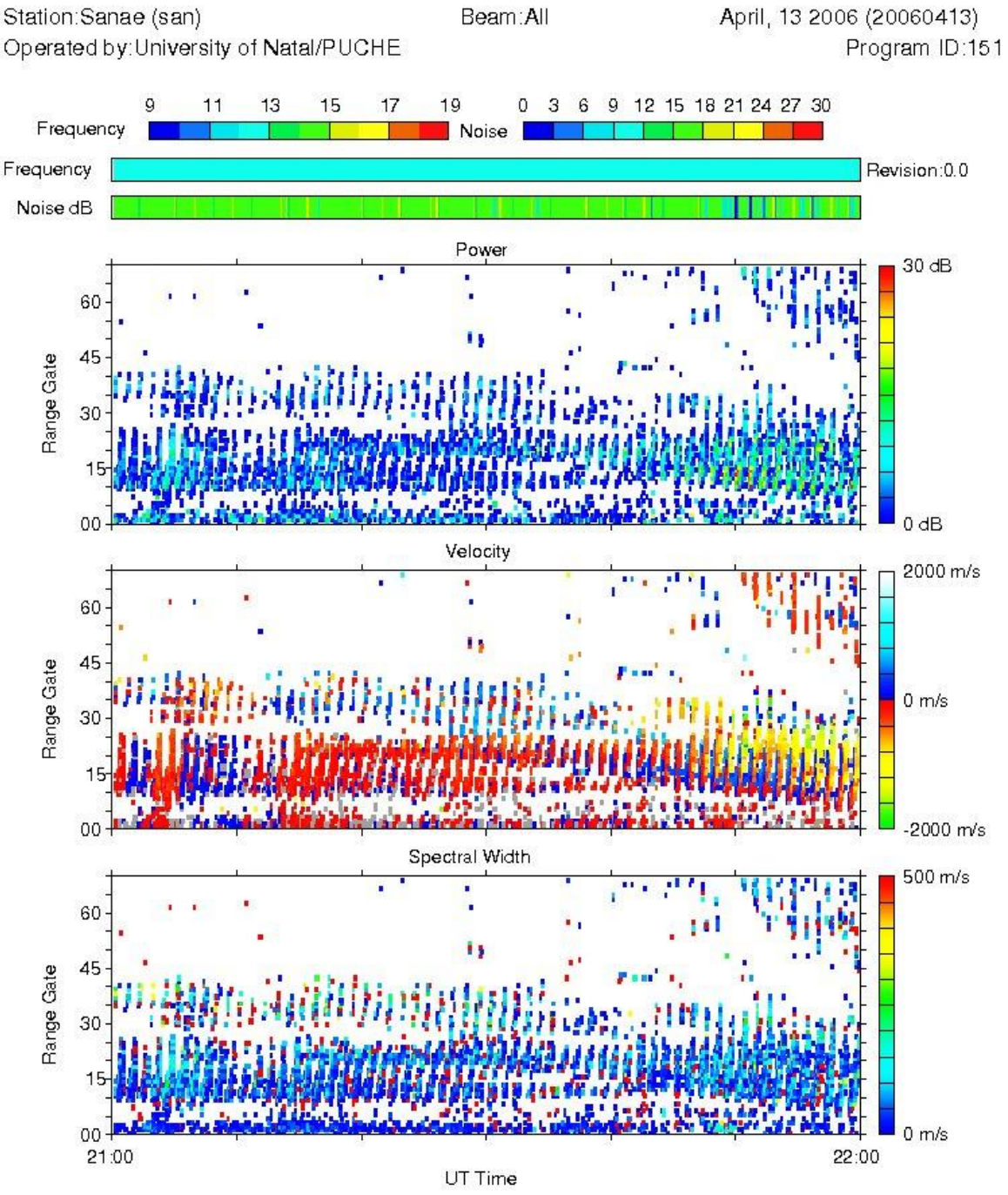

In the middle panel, the line-of-sight Doppler velocities were predominantly away from the radar from 21:00 to 21:45 UT, which corresponds with anti-sunward flows, typical for this magnetic local time. There is a short increase in velocity with a flow burst from approximately 21:45 to 22:00 UT, moving away from the radar.

(d) Tiger radar from southern hemisphere

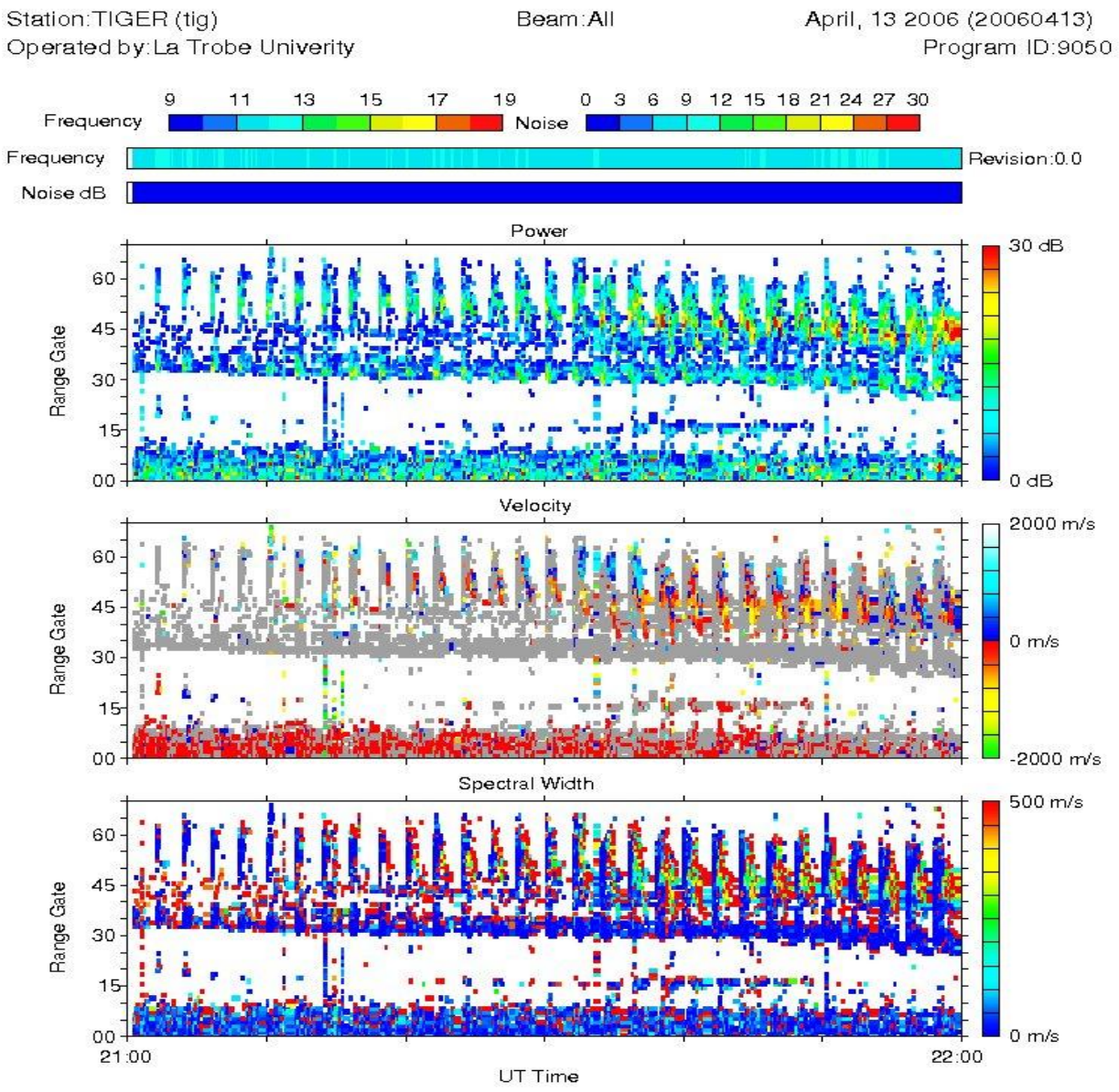

In the middle panel, below range gate 15, the dominating plasma flow is away from the radar. There is a short period increase in velocity with a flow burst from 21:30 to 21:50 UT, which also variable with time, above range gate 40.

4.6 Evidence for non-substorm interval

Figs. 4.10 and 4.11 present the IMAGE magnetometer data for x -components of the magnetic field in both intervals. The highlighted grey vertical lines represent interval1 on the 07 April 2006 (02:10 – 03:10 UT) in Fig. 4.10 and interval 2 on the 13 April 2006 (21:00 – 22:00 UT) in Fig. 4.11. In interval 1, during this day the geomagnetic activity was very quiet, as shown in the previous section. In interval 2, the geomagnetic activity was quiet even prior to the period of interest, but later there are signatures of substorms. These plots in both intervals show no evidence of substorms in the period of interest. We had examined the other components of the magnetic field they are quite similar. We chose to display one component of the magnetic field for each interval.

4.6.1 Interval 1: 07 April 2006 (02:10 – 03:10 UT)

X -component of the magnetic field

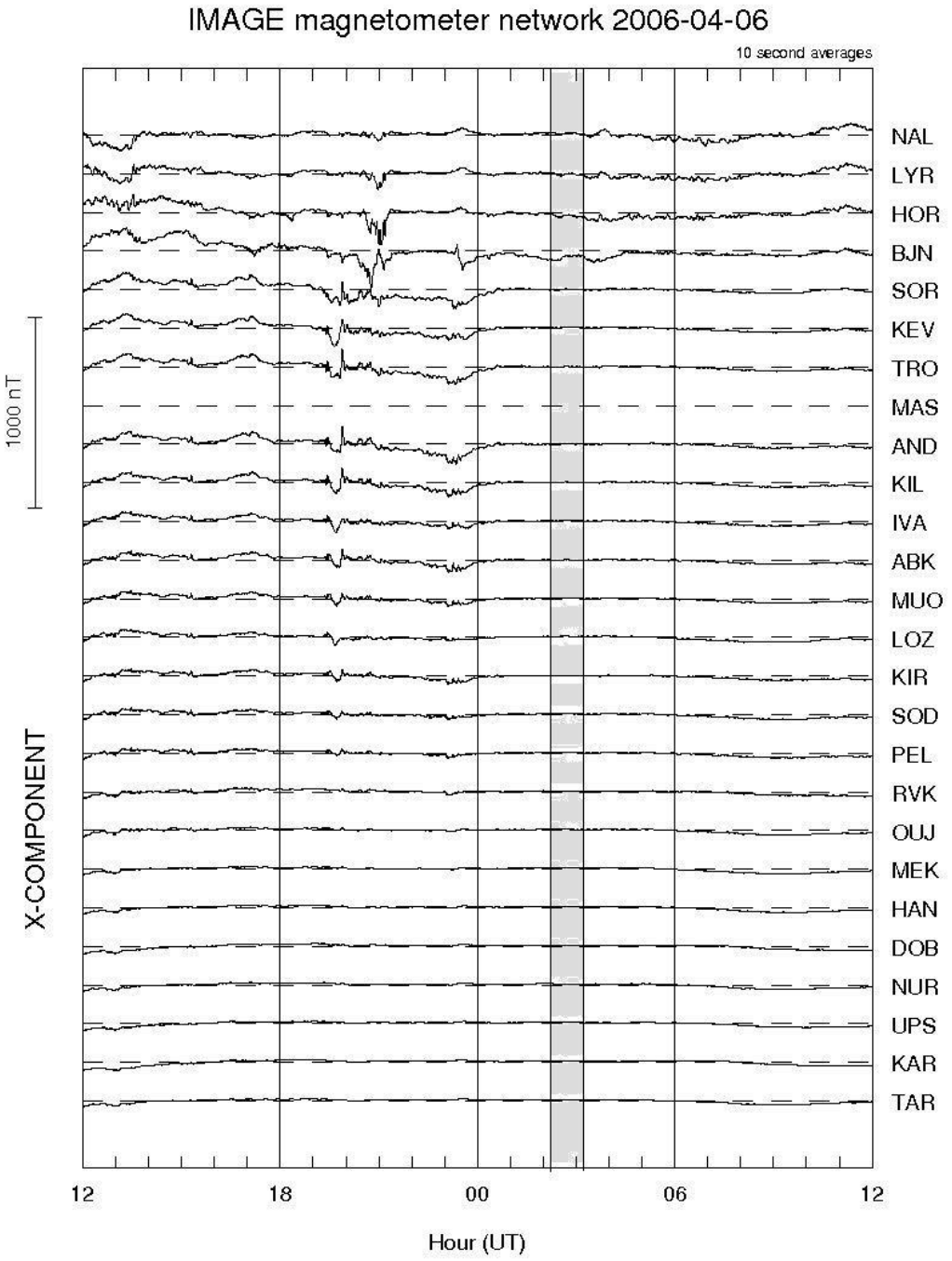

Fig. 4.10: IMAGE magnetometer network shows no substorm activity for the three (x, y and z) components of the magnetic field (adapted from http://www.ava.fmi/image/reqform/dataform.html).

4.6.2 Interval 2: 13 April 2006 (21:00 – 22:00 UT)

X -component of the magnetic field

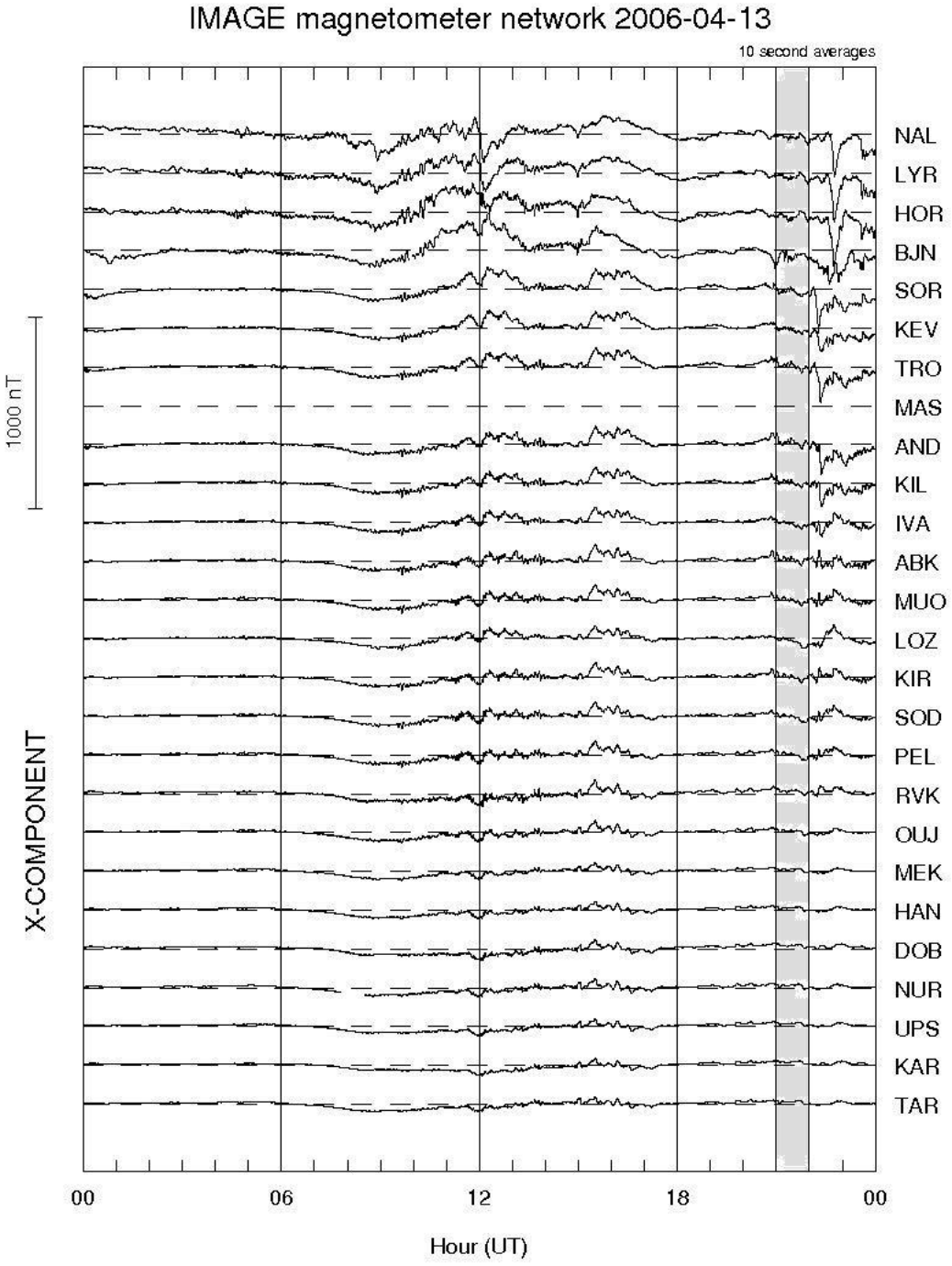

Fig. 4.11: IMAGE magnetometer network shows no substorm activity for the three (x, y and z) components of the magnetic field (adapted from http://www.ava.fmi/image/reqform/dataform.html).

4.7 Consistent with TRINNIs

Figs. 4.12 and 4.13 show 24-hour plots of Pi2 pulsations from Hermanus Magnetic Observatory (34^0 25'27"S, $19^0$13'29"E). The solid vertical lines in Fig. 4.12 represent interval 1 on 07 April 2006 and in Fig. 4.13 represent interval 2 on 13 April 2006. From the Pi2 plots in the period of interest, there are no significant indications of substorms. No substorm activity was observed in association with these flow bursts. We have looked at IMAGE magnetometer data in the above figures, and found no evidence of substorms during the periods of interest. Sutcliffe (2010) has shown that Pi2s which may occur during quiet times have slightly different properties than those which occur at substorm onset. It would appear that the Pi2s which we have observed during the periods of interest are of the first ('quiet') type, and Sutcliffe has shown that these are not always present. Thus observations of Pi2s during the periods of interest are not inconsistent with the absence of substorms, since we are not observing 'substorm type' Pi2s. Sutcliffe (2010) has suggested that Pi2s may be more generally associated with pulsed reconnection, which is what occurs in association with flow bursts during quiet times, and in a different way with the onset of substorms. Normally Pi2s are associated with substorms, but can also occur in association with TRINNIs (Sutcliffe, 1998; Sutcliffe & Lyons, 2002).

4.7.1 Interval 1: 07 April 2006 (02:10 – 03:10 UT)

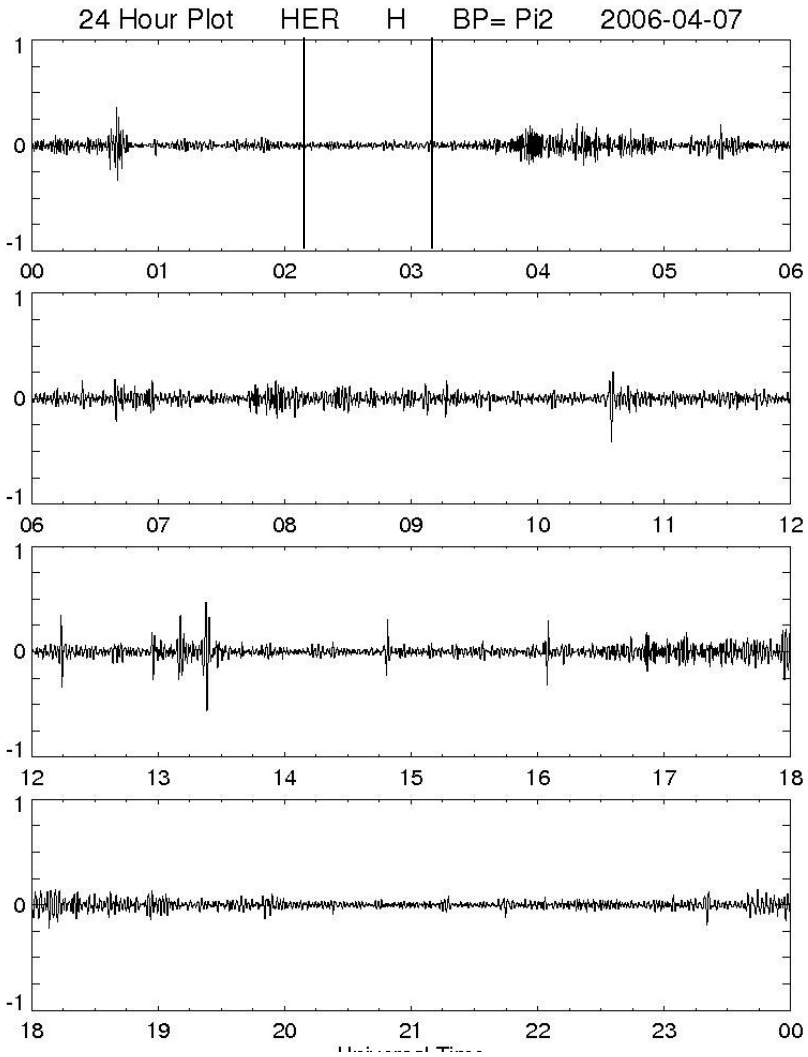

Fig. 4.12: Pi2 pulsations for interval 1 generated at Hermanus Magnetic Observatory, period of interest on 07 April 2006 (02:10 – 03:10 UT).

4.7.2 Interval 2: 13 April 2006 (21:00 – 22:00 UT)

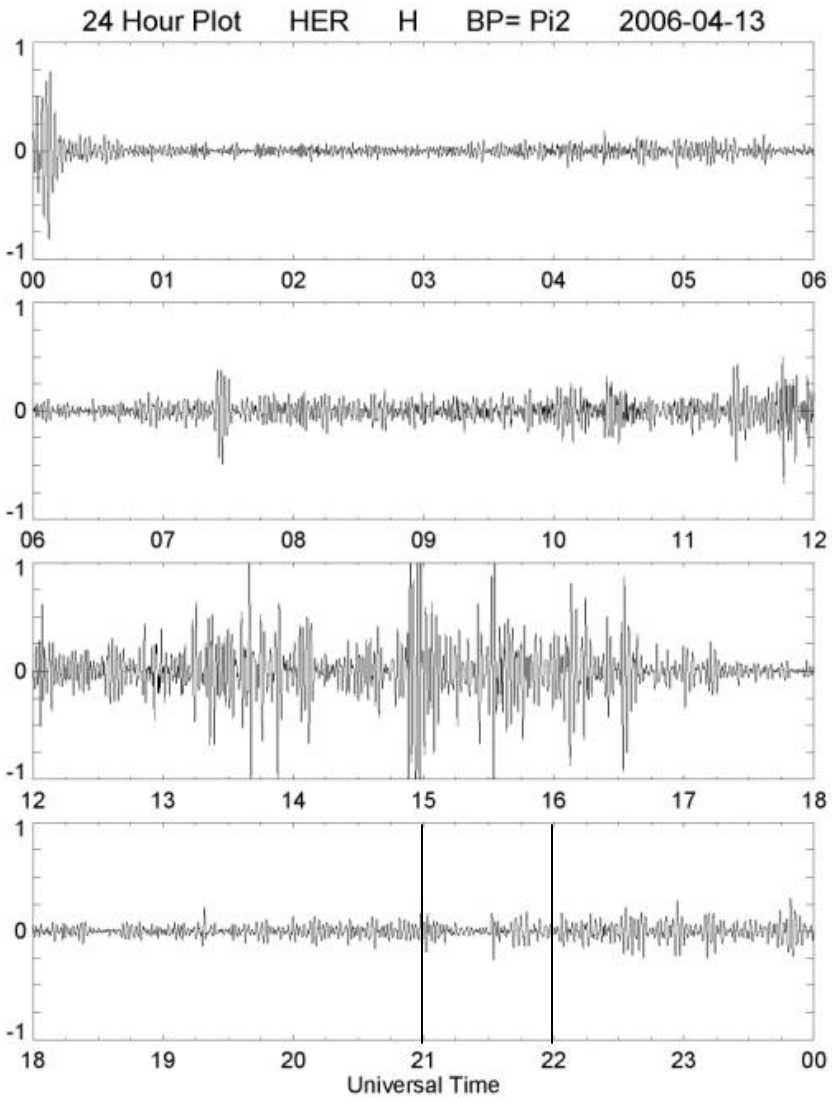

Fig. 4.13: Pi2 pulsations for interval 1 generated at Hermanus Magnetic Observatory, period of interest on 13 April 2006 (21:00 – 22:00 UT).

These Pi2 pulsations were observed during the intervals of quiet geomagnetic conditions which are similar to those reported by Sutcliffe and Lyons (2002). These authors observed that several Pi2 bursts occurred simultaneously at high (magnetic latitude=71°) and lower (42°) latitude during the absence of magnetospheric substorms.

4.8 Particle time series plots

Figs. 4.14 and 4.15 present the time series plots for electrons and protons measured on the GOES satellites. We used GOES 12, 10 satellites for electrons and GOES 10, 11 satellites for protons in both intervals. We omitted GOES-11 satellite for electrons because this satellite is in storage mode and spinning. Therefore the electron fluxes vary with the spin of the spacecraft, and the flux can be easily be misinterpreted. In the figures, the highlighted grey vertical lines represent interval 1 on 07 April 2006 and interval 2 on 13 April 2006. These time series plots show no evidence of geomagnetic storms, which would be accompanied by increased fluxes of energetic particles, particularly in the period of interest.

4.8.1 Interval 1: 07 April 2006 (02:10 – 03:10 UT)

Fig. 4.14: Particle measurements for flux of E > 2 MeV electrons and E > 1 MeV protons on GOES satellite for 1 minute on interval 1 (adapted from http://spidr.ngdc.noaa.gov/).

(a) GOES -12 electron > 2 MeV

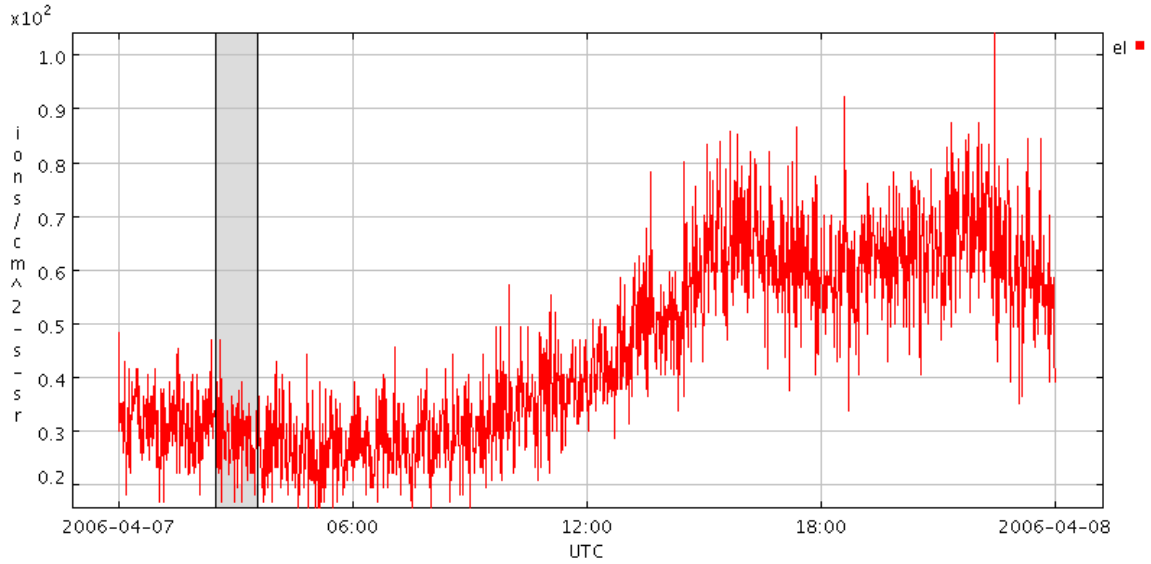

The electron flux is less than 0.5 x10^2 ions/cm^2 s sr, which shows that the particles show no signatures of geomagnetic storms.

(b) GOES 10 Proton > 1 MeV

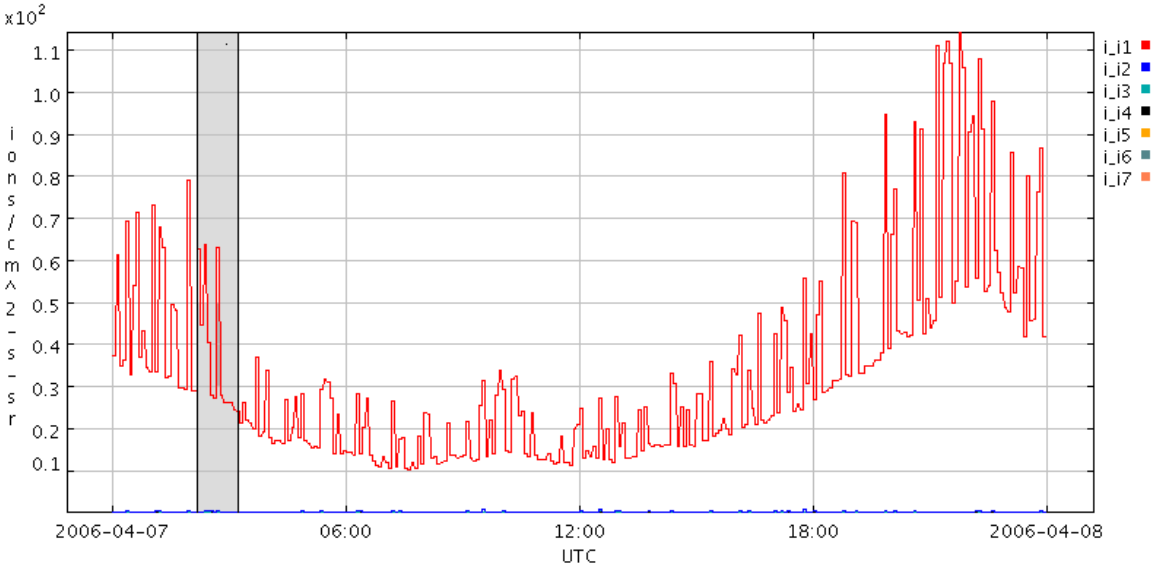

The corrected proton fluxes of E > 1 MeV, measured by GOES-10 satellite. The flux is low, less than 0.8 x10^2 ions/cm^2 s sr. This magnitude of flux is an indication of quiet geomagnetic activity.

4.8.2 Interval 2: 13 April 2006 (21:00 – 22:00UT

Fig. 4.15: Particle measurements for flux of E > 2 MeV electrons and E > 1 MeV protons on GOES satellite for 1 minute on interval 2 (adapted from http://spidr.ngdc.noaa.gov/).

(a) GOES -12 electron > 2 MeV

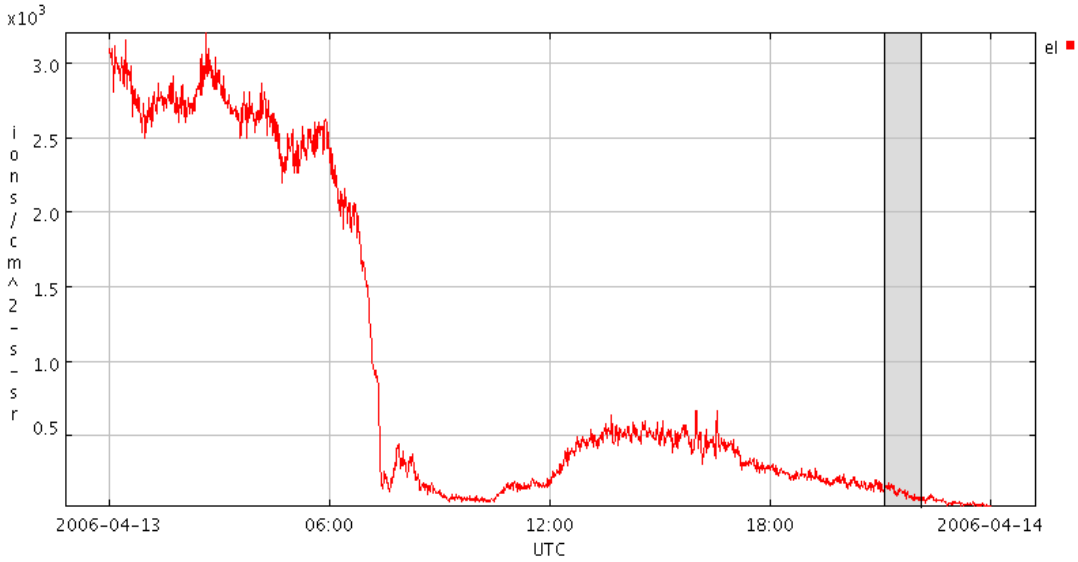

The electron flux is less than 0.3x10^3 ions/cm^2 s sr, which shows that the particles show no signatures of geomagnetic storms.

(a) GOES 10 Proton > 1 MeV

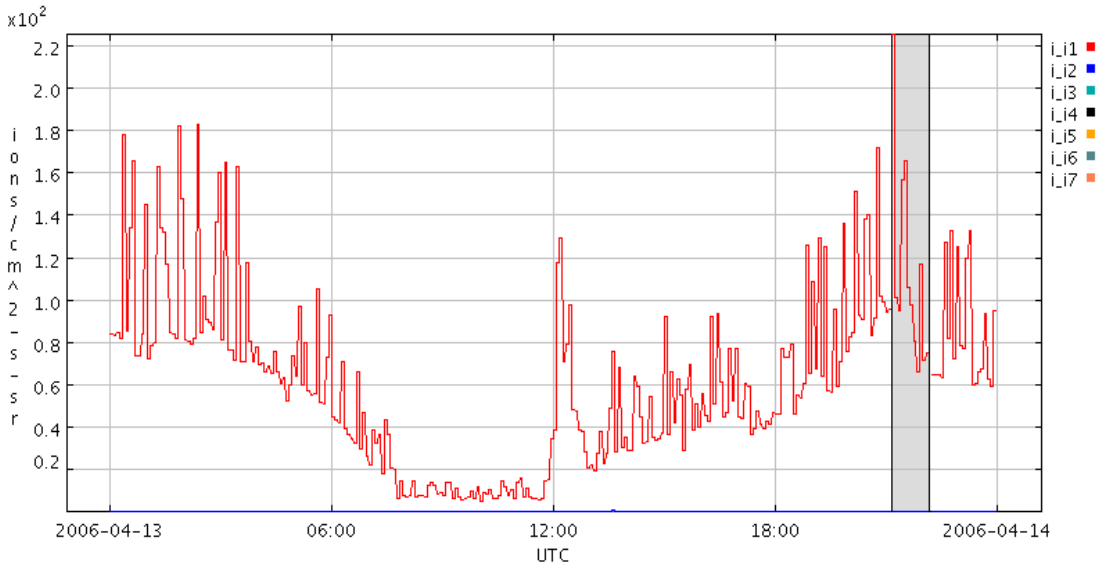

The corrected integral proton flux had a sudden increase in magnitude at 21:00 but remained below 2.3 x10^2 ions/cm^2 s sr. This low magnitude of the flux signifies quiet geomagnetic activity. The proton flux of E > 1 MeV measured by GOES 10 satellites.

The electron flux as recorded by GOES satellites 12 and 10, are quite similar and the proton flux as recorded by GOES satellites 10 and 11 are also quite similar with their magnitudes, but all of them are at different longitudes, we took one of them for illustration.

CHAPTER 5

DISCUSSION

5.1 Significance of the IMF orientation

The interplanetary magnetic field conditions confirmed that the B_z –component of the IMF at the dayside of the magnetopause was northwards in both intervals, but with a significant positive B_y – component in interval 1 on 07 April 2006 and negative B_y –component for interval 2 on 13 April 2006. In both intervals B_y strong dominated the B_z -component of the Interplanetary magnetic field.

The results have shown the occurrence of nightside flow bursts with a strongly B_y –component influenced interplanetary magnetic field. These flow bursts are likely consistent with previous observations of tail reconnection during IMF northward non-substorm intervals. The tendency to occur when the interplanetary magnetic field is northward suggests an association with non-substorm intervals. The assumption of a non-substorm intervals in this study have been justified by the use of IMAGE magnetometer data, Pi2 pulsations and GOES satellite data.

5.2 Pi2 pulsations

Pi2 pulsations have been traditionally observed at the breakup of a magnetospheric substorm. The Pi2 pulsation is the one of the most common forms of pulsation used in substorm studies. On the other hand, Pi2 pulsations are believed to be dependent on solar wind velocity and the B_z – component of the interplanetary magnetic field (Sobolev et al., 1994). Sutcliffe (1998, 2002) has shown that Pi2 pulsations sometimes occur in unusual conditions with which they had not previously been associated, namely extremely quiet solar wind and magnetospheric conditions. In these periods there were no significant signatures of substorm activity. In the results, Pi2 plots show no evidence of substorm activity in the period of interest in both intervals.

These flow bursts suggest that at least in some cases tail reconnection during IMF northward non-substorm intervals may occur in association with Pi2 pulsations during quiet periods.

5.3 GOES satellite particle measurements

The Geostationary Operational Environment Satellites (GOES) system provides continuous monitoring of, amongst others, particles at geostationary orbit. We used GOES satellite data for energetic particles as an additional check for substorms. In both intervals, we observed that the particle events shown in the plots in Fig. 4.15 and 4.16 showed no evidence of accompanying geomagnetic storms. This indicates that the particle event does not necessarily occur in association with a geomagnetic storm. The particle results have shown evidence of quiet geomagnetic activity, which is normally expected with no significant southward turning of IMF B_z and no disturbance in the inner magnetosphere in both intervals. The low incidence of energetic particles during the two intervals of interest confirmed that both intervals can be characterized as non-substorm, thus confirming the observation in section 5.1 that flow bursts occur during non-substorm interval when the magnetic field is northward.

5.4 High-latitude ionospheric convection patterns

The high latitude ionospheric convection patterns are determined by magnetic reconnection at the magnetopause and in the tail. The consequences of magnetic flux transfer from dayside to the nightside due to reconnection at the magnetopause and from the transfer of flux from nightside to the dayside at lower latitudes as the results of nightside reconnection in the magnetotail lead to high-latitude ionospheric convection. When the interplanetary magnetic field is northward, the IMF reconnects with lobe field lines at high-latitude in the tail of the magnetosphere, called high-latitude reconnection. This mechanism causes the solar wind plasma and energy to penetrate the magnetosphere. The results have shown that the presence of strong B_y –component dominating the B_z -component of the IMF in both intervals led to asymmetry of the convection patterns. This is in agreement with the well known statement that the interplanetary magnetic field plays a significant role in controlling the nature of convection in the magnetosphere and ionosphere.

5.5 Flow bursts magnitude

These flow bursts were observed during geomagnetic quiet periods with a northward IMF, although B_y was dominating the B_z -component throughout both intervals. In interval 1, the magnitudes of the flow velocities during B_y positive are lower than the magnitudes of the flow velocities during B_y negative in interval 2. This is useful to illustrate a relationship between the nightside dynamics and the prior dayside activity. The magnitude of the Interplanetary magnetic field components for B_x, B_y and B_z were larger during B_y negative in interval 2. It means that the high rate of dayside reconnection which would be expected to occur in the presence of a stronger IMF (Freeman et al., 1993) might reasonably be expected to lead to intense tail driven convection.

5.6 Tail reconnection

These flow bursts are interpreted as being associated with magnetic reconnection. Reconnection in the tail is often associated with substorm break-up, which closes open flux and causes the polar cap to contract. The appearance and development of the break-up aurora is associated with substorms. It is also observed that there are intervals of tail reconnection that are not associated with the classic signatures of substorms (Grocott et al., 2003, 2004, 2005; Milan et al., 2005).

Fig. 5.1 shows a schematic diagram for high-latitude reconnection. During northward IMF, reconnection may occur at higher latitudes (Dungey, 1963). Fig. 5.1 illustrates that the high-latitude reconnection ($\mathbf{N_1}$) takes place between interplanetary field lines (red lines) without connection to the Earth and lobe field lines, which are connected to the Earth at one side (black lines).

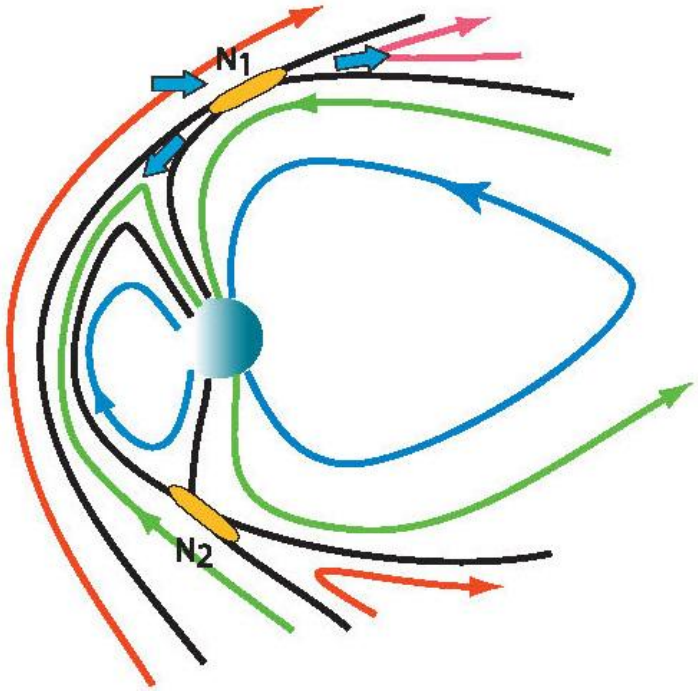

Fig. 5.1: Schematic diagram for high-latitude reconnection for northward IMF (from Dorelli et al., 2007)

After reconnection, the newly connected field lines have the same topology, so that there is no net flux transfer between the two regions (Reiff & Burch, 1985). Later, the newly connected lobe field lines are dragged toward the tail and may again reconnect with another lobe field line.

The IMF has an anti-sunward component in addition to the northward component for interval 1. In this case, as shown in Fig. 5.1, high-latitude reconnection takes place first in the northern hemisphere (**N_1**), followed by reconnection in the southern hemisphere (**N_2**). For interval 2, the IMF has a sunward component in addition to the northward component. In this case, the high-latitude reconnection takes place first in the southern hemisphere followed by reconnection in the northern hemisphere. These nightside flow bursts have revealed that, for northward IMF, reconnection can occur in the magnetotail instead of at the front of the magnetosphere.

CHAPTER 6

CONCLUSION

The study presented SuperDARN, IMAGE magnetometer, Hermanus pulsation magnetometer and GOES satellite observations when the interplanetary magnetic field was northward but B_y –strongly dominated the B_z –component of the IMF. In looking at the generated outputs for ionospheric convection patterns, radar time series plots and radar field-of-view from SuperDARN HF radars in this study, we observed convection patterns and localized flow bursts similar to those obtained by Grocott et al (2007) and others. The data from IMAGE magnetometers, Hermanus pulsation magnetometers and GOES satellites confirmed that the flow bursts observed in this study were not associated with substorm activities.

This study has shown the occurrence of nightside flow bursts which occur during intervals of northward but strongly B_y –influenced interplanetary magnetic field. These bursts of flow in the nightside high latitude ionosphere have been associated with TRINNIs. The results presented above also indicate that the nightside ionospheric flows for northward IMF with B_y –positive also occur when B_y is negative. It is also found that, in this case when IMF B_y is negative the nightside ionospheric convection is stronger than when B_y is positive. This study has further shown that the direction of the high speed flows (flow bursts) and underlying convection pattern is governed by the orientation of B_y, implying that the tail dynamics responsible for driving them are also directly related to the nature of the interplanetary magnetic field. The results discussed above and results from the previous studies mentioned in chapter 3 for the nightside ionosphere and geomagnetic tail were observed during intervals of northward IMF and quiet geomagnetic activity.

Hence these observed flow bursts can be associated with reconnection in the tail. From the figures of ionospheric convection patterns for total cross polar cap potential (CPCP), we estimate the rate of tail reconnection as between 35 -65 kV during non-substorm intervals. (The rate of magnetic reconnection in Wb/s is conventionally expressed in kV through Faraday's law).

Sutcliffe (2010) has investigated several occurrences of Pi2s during quiet periods, including TRINNIs. The period studied here are further examples of tail reconnection during IMF northward non-substorm interval (TRINNI) events.

6.1 Possible future work

In terms of the future work regarding improvements to the results obtained in this study: further study is needed to investigate many more northward IMF intervals during quiet periods. We suggest that the B_y -component must not too strong as compared to the B_z -component of the IMF, although it should be dominating because this leads to convection patterns which are not well defined.

Further study is needed to confirm an association of tail reconnection during IMF northward non-substorm interval (TRINNI) occurrence with Pi2 pulsations during quiet periods. We hope that this will also lead to discovering if there is any relationship between TRINNI events and poleward boundary intensifications (PBIs), since Pi2 pulsations are associated with poleward boundary intensifications during the absence of substorms (Sutcliffe, 2002; Kim, 2005). It would also be of interest to find similar events where lower latitude radars (for example Wallops or Hokkaido) have data, so that the latitude of the Heppner-Maynard boundary can be more accurately determined.

REFERENCES

Ambrosino D., Amata E., Marcucci M.F., Coco I., Bristow W. and Dyson P., "Different responses of northern and southern high latitude ionospheric convection to IMF rotations: a case study based on SuperDARN observations", *Annales Geophysicae*, **27**, 2423-2438, 2009.

Biskamp D., "Magnetic substorms" in *Magnetic reconnection in Plasmas*, edited by Biskamp D, p. 320, Cambridge Monographs on Plasma Physics 3, 2000.

Burgess D., "Collisionless shocks" in *Introduction to Space Physics*, edited by Kivelson M.G. and Russell C., *p. 129* , Cambridge University Press, Cambridge 1995.

Chisham G., Lester M., Milan S.E., Freeman M.P., Bristow W.A., Grocott A., McWilliams K.A., Ruohoniemi J.M., Yeoman T.K., Dyson P.L., Greenwald R.A., Kikuchi T., Pinnock M., Rash J.P.S., Sato N., Sofko G.J., Villain J.P., and Walker A.D.M., "A decade of the Super Dual Auroral Radar Network (SuperDARN): scientific achievements, new techniques and future directions", *Surveys of Geophysics*, **28**, 33-109, 2007.

Dorelli J.C., Bhattacharjee A. and Raeder J., "Separate reconnection at Earth's dayside magnetopause under generic northward interplanetary magnetic field conditions", *Journal of Geophysical Research*, **112**, (A02202), doi: 10.1029/2006JA011877, 2007.

Dungey J.W., "The Structure of the Exosphere or Adventures in the Velocity Space*", Geophysics of the Earth's Environment,* edited by Dewitt C., Hieblot J. and Le Beau A., Gordon and Breach, New York 505-550, 1963.

Finn J.M., "Magnetic reconnection null point", *Nature Physics*, **2**, 445-446, 2006.

Freeman M.P., Farrugia C.J., Burlaga L.F., Hairston M.R., Greenspan M.E., Ruohoniemi J.M. and Lepping R.P., "The Interaction of a Magnetic Cloud with the Earth: Ionospheric Convection in the Northern and Southern Hemispheres for a Wide Range of Quasi-Steady Interplanetary Magnetic Field Conditions", *Journal of Geophysical Research*, **98**, (A5), 7633-7655, 1993.

Greenwald R.A., Baker K.B., Dudeney J.R., Pinnock M., Jones T.B., Thomas E.C., Villain J.P., Cerisier J.C., Senior C., Hanuise C., Hunsucker R.D., Sofko G., Koehler J., Nielsen E., Pellinen R., Walker A.D.M., Sato N. and Yamagishi H., "A Global View of the Dynamics of High-Latitude Convection", *Space Science Reviews*, **71**, 761-796 , 1995.

Grocott A., Cowley S.H.W. and Sigwarth J.B., "Ionospheric flow during extended intervals of northward but B_Y-dominated IMF", *Annales Geophysicae*, **21**, 509-538, 2003.

Grocott A., Badman S.V., Cowley S.W.H., Yeoman T.K. and Cripps P.J., "The influence of IMF B_Y on the nature of the nightside high-latitude ionospheric flow during intervals of positive B_Z ", *Annales Geophysicae,* **22**, 1755-1764, 2004.

Grocott A., Yeoman T.K., Milan S.E. and Cowley S.W.H., "Interhemispheric observations of the ionospheric signature of tail reconnection during IMF-northward non-substorm intervals", *Annales Geophysicae*, **23**, 1763-1770, 2005.

Grocott A., Yeoman T.K., Milan S.E., Amm O., Frey H.U., Juusola L., Nakamura R., Owen C.J., Rème H. and Takada T., "Multi-scale observations of magnetotail flux transport during IMF-northward non-substorm intervals", *Annales Geophysicae*, **25**, 1709-1720, 2007.

Heppner J.P. and Maynard N.C., "Empirical High-latitude Electric Field Models", *Journal of Geophysical Research*, **92**, (A5), 4467-4489, 1987.

Hu H., Yeoman T.K., Lester M., Liu R., Yang H. and Grocott A., "Dayside flow bursts and high-latitude reconnection when the IMF is strongly northward", *Annales Geophysicae*, **24**, 2227-2242, 2006.

Hughes W.J., "The magnetopause, magnetotail, and magnetic reconnection" in *Introduction to Space Physics*, edited by Kivelson M.G. and Russell C., p. 227, Cambridge University Press, Cambridge 1995

Kim K.H., Takahashi K., Lee D.H., Sutcliffe P.R. and Yumoto K., "Pi2 pulsations associated with poleward boundary intensifications during absence of substorms", *Journal of Geophysical Research* **110**, (A01217), doi: 10.1029/2004JA010708, 2005.

Lockwood M. and Moen J., "Reconfiguration and closure of lobe flux by reconnection during northward IMF: possible evidence for signatures in cusp/cleft auroral emissions", *Annales Geophysicae*, **17**, 996-1011, 1999.

McComas D.J., Bame S.J., Barker P., Feldman W.C., Philips J.L., Riley P. and Griffee J.W., "Solar Wind Electron Proton Alpha Monitor (SWEPAM) for the Advanced Composition Explorer", *Space Science Reviews,* **86**, 563-612, 1998.

Milan S.E., Hubert B. and Grocott A., "Formation and motion of a transpolar arc in response to dayside and nightside reconnection", *Journal of Geophysical Research*, **110**, (A01212), doi: 10.1029/2004JA010835, 2005.

Nishida A., Mukai T., Yamamoto T., Kokubun S. and Maezawa K., "Unified model of the magnetotail convection in geomagnetically quiet and active times", *Journal of Geophysical Research*, **103**, (A3), 4409-4418, 1998.

Reiff P.H. and Burch J.L., "IMF B_Y-dependent plasma flow and birkeland currents in the dayside magnetosphere 2. A global model for northward and southward IMF", *Journal of Geophysical Research*, **90**, (A2), 1595-1609, 1985.

Rostoker G., Akasofu S.-I., Foster J., Greenwald R. A., Kamide Y., Kawasaki K., Lui A. T. Y., McPherron R. L. and Russell C. T., "Magnetospheric Substorms—Definition and Signatures", *Journal of Geophysical Research*, **85**, (A4), 1663–1668, 1980.

Ruohoniemi J.M. and Greenwald R.A., "Statistical patterns of high-latitude convection obtained from Goose Bay HF observations", *Journal of Geophysical Research*, **101**, (A10), 21743-21763, 1996.

Ruohoniemi J.M. and Baker K.B., "Large-scale imaging of high-latitude convection with Super Dual Auroral Radar Network HF radar observations", *Journal of Geophysical Research*, **103**, 20797-20811, 1998.

Russell L.C. and Luhmann J.G., "Earth: Magnetic field and magnetosphere", in *Encyclopedia of Planetary Sciences*, edited by Shirley J.H. and Fainbridge R.W., 208-211, Chapman and Hall, New York, 1997.

Sandholt P.E., Farrugia C.J., Moen J., Noraberg Ø., Lybekk B., Sten T. and Hansen T., "A classification of dayside auroral forms and activities as a function of interplanetary magnetic orientation", *Journal of Geophysical Research*, **103**, (A10), 23325-23345, 1998.

Senior C., Cerisier J.C., Rich F., Lester M. and Parks G.K., "Strong sunward propagating flow bursts in the nightside sector during quiet solar wind conditions: SuperDARN and satellite observations", *Annales Geophysicae*, **20**, 771-779, 2002.

Shepherd S.G. and Ruohoniemi J.M., "Electrostatic potential patterns in the high-latitude ionosphere constrained by SuperDARN measurements", *Journal of Geophysical Research*, **105**, (A10), 23005-23014, 2000.

Smith C.W., L'Heureux J., Ness N.F., Acuña M.H., Burlaga L.F. and Scheifele J., "The ACE Magnetic Field Experiment", *Space Science Reviews*, **86**, 613-632, 1998.

Sobolev A.V., "Dependence of irregular geomagnetic Pi2 pulsations on parameters of the interplanetary magnetic field", *Geomagnetism and Aeronomy*, English translation, **34**, (2)*,* 1994.

Stone E.C., Frandsen A.M. and Mewaldt Christian E.R., Margolies D., Ormes J.F and Snow F., "The Advanced Composition explorer", *Space Science Reviews*, **86**, 1-22, 1998.

Sutcliffe P.R., "Observations of Pi2 pulsations in a near ground state magnetosphere", *Geophysical Research Letters*, **25**, (21), 4067-4070, 1998.

Sutcliffe P.R. and Lyons L.R., "Association between quiet-time Pi2 pulsations, poleward boundary intensifications, and plasma sheet particle fluxes", *Geophysical Research Letters*, **29**, (9), 1293, 10.1029/2001GL014430, 2002.

Sutcliffe P.R., "Pi2 band activity at low latitudes during non-substorm intervals", *Geophysical Research Letters,* **37**, L05101, doi:10.1029/2009GL041661, 2010.

Walker A.D.M, Greenwald R.A. and Baker K.B., "Determination of the level of ionospheric irregularities from radar backscatter measurements", *Radio Science*, **22**, 689-705, 1987.

Walker A.D.M., Pinnock M., Baker K.B., Dudeney J.R. and Rash J.P.S., "Strong flow bursts in the nightside ionosphere during extremely quiet solar wind conditions", *Geophysical Research Letters* **25**, (6), 881-884, 1998.

Walker A.D.M., Baker K.B., Pinnock M., Dudeney J.R. and Rash J.P.S., "Radar observations of magnetospheric activity during extremely quiet solar wind conditions", *Journal of Geophysical Research* **107**, (A4), 1038, 10.1029/2001JA000063, 2002.

Watanabe M., Sofko G.J., Kabin K., Rankin K, Ridley A. J., Clauer C.R. and Gombosi T.I., "Origin of the interhemispheric potential mismatch of merging cells for interplanetary magnetic field B_y – dominated periods", *Journal of Geophysical Research*, **112**, (A10205), doi: 10.1029/2006JA012179, 2007.

Wolf R.A., "Magnetospheric configuration" in *Introduction to Space Physics*, edited by Kivelson M.G. and Russell C., *p. 288*, Cambridge University Press, Cambridge 1995.